Journal of Biomolecular NMR, 9 (1997) 371–388

J-Bio NMR 433

Unambiguous NOE assignments in proteins by a combination of through-bond and through-space correlations

Frank Löhr and Heinz Rüterjans*

Institut für Biophysikalische Chemie, Johann Wolfgang Goethe Universität Frankfurt am Main, Biozentrum N230, Marie-Curie-Strasse 9, D-60439 Frankfurt, Germany

Received 21 October 1996
Accepted 28 January 1997

Keywords: Triple-resonance NOESY; Resonance assignments; Degenerate chemical shifts; *Desulfovibrio vulgaris* flavodoxin

Summary

Heteronuclear editing has found widespread use in the detection of proton–proton dipolar interactions in isotopically labelled proteins. However, in cases where both the resonances of protons and directly bound ^{13}C or ^{15}N spins of two or more sites are degenerate, unambiguous assignments are difficult to obtain by conventional methods. Here, we present simple extensions of well-known triple-resonance pulse sequences which improve the dispersion of NOESY spectra. In order to record the chemical shifts of backbone nuclei which allow a resolution of overlapping cross peaks, the magnetization is relayed via the scalar coupling network either before or after the NOE mixing period. The novel pulse sequences are applied to flavodoxin from the sulfate-reducing organism *Desulfovibrio vulgaris*. A number of previously unassigned NOE interactions involving α-, β- and amide protons can be unequivocally identified, suggesting that the accuracy of protein structure determination can be improved.

Introduction

The introduction of triple-resonance pulse sequences (Ikura et al., 1990; Kay et al., 1990b; Montelione and Wagner, 1990) has greatly facilitated the resonance assignment of polypeptides. While the magnitude of one-bond scalar couplings allows the application to proteins with comparatively broad lines, their uniformity makes the identification of intra- and interresidual correlations virtually independent of local conformations. An advantage inherent to the 'classical' sequential assignment strategy (Wüthrich, 1986; Marion et al., 1989a,b; Zuiderweg and Fesik, 1989), namely the additional recognition of secondary structure elements based on characteristic NOE patterns, is however lost, although some information can already be revealed from ^{1}H and ^{13}C chemical shifts themselves using the Chemical Shift Index (Wishart and Sykes, 1994). On the other hand, many triple-resonance experiments provide more than sufficient signal-to-noise ratios even for moderately concentrated samples, especially when applied at the highest field strengths currently commercially available (750 MHz, 800 MHz). Therefore, it can be envisaged to retain the information about dipolar interactions during the process of resonance assignment with the latter relying exclusively on through-bond correlations. The strategy proposed here combines well-known triple-resonance techniques with the magnetization transfer via $^{1}H,^{1}H$ NOEs.

Previously, editing by nitrogen or carbonyl chemical shifts was already employed in order to resolve overlapping correlations in the scalar coupling network of the side chains using triple-resonance relay methods such as HC(C)(CO)NH-TOCSY (Montelione et al., 1992; Clowes et al., 1993; Grzesiek et al., 1993; Logan et al., 1993), HC(C)NH-TOCSY (Lyons and Montelione, 1993) or HCACO-TOCSY (Kay et al., 1992a), to name only a few. An important aspect of triple-resonance NOESY experiments presented in this paper is the improved dispersion of NOE cross peaks when compared to homonuclear or conventional heteronuclear edited NOESY experiments. NOEs involving degenerate protons are not only separated by the chemical shifts of directly bound heteronuclei

*To whom correspondence should be addressed.

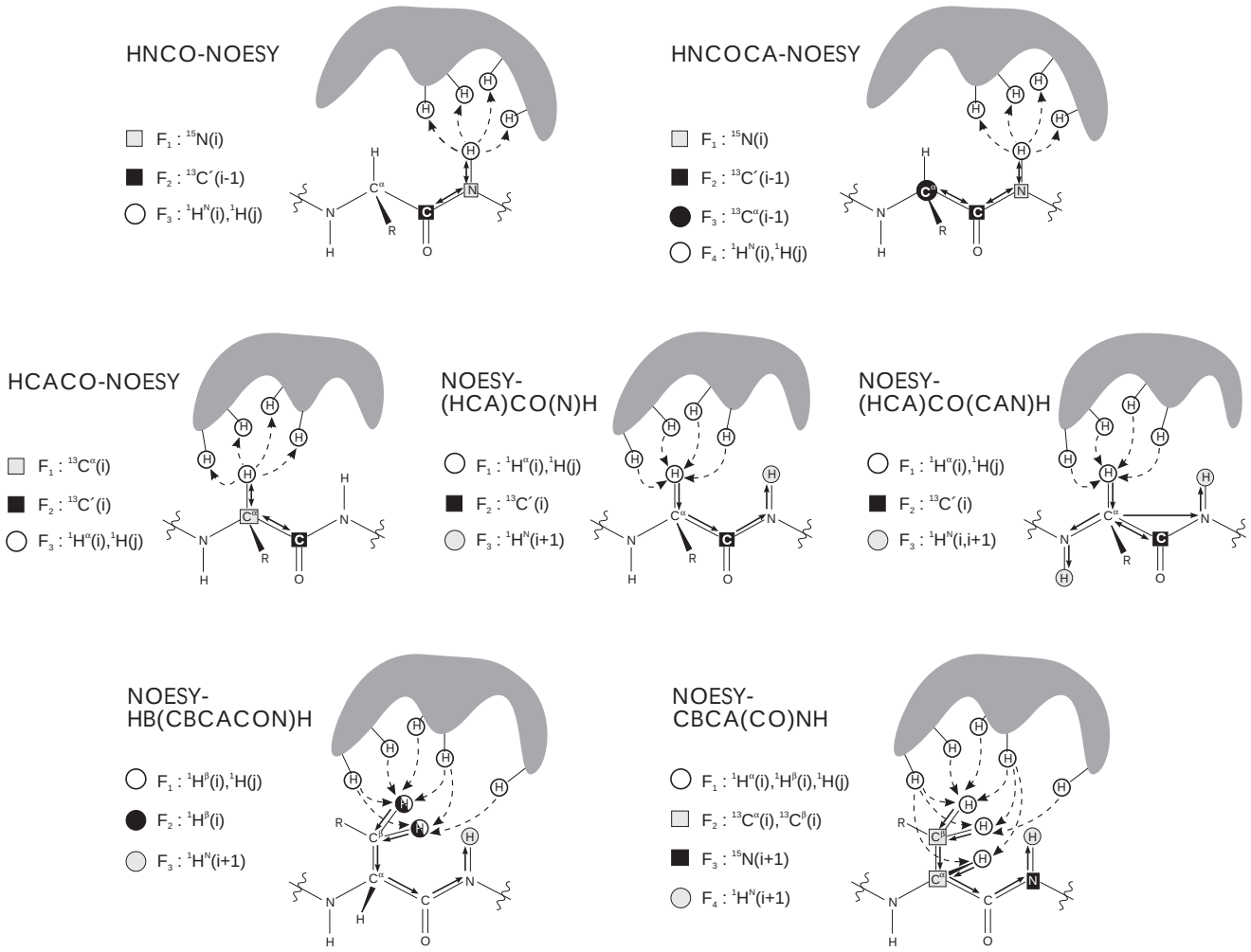

Fig. 1. Schematic representation of the magnetization transfer pathways induced by the various triple-resonance NOESY pulse sequences. Straight arrows indicate a transfer via scalar couplings while broken curved arrows represent dipolar interactions. The detectable NOEs involve amide protons (top), α-protons (middle) and β-protons (bottom).

but also by the chemical shifts of further protein backbone spins, e.g. $^{13}C'$ or, in the case of aliphatic protons, ^{15}N and $^{1}H^{N}$. If both the proton and the heteronucleus of two or more CH or NH groups exhibit identical resonance frequencies – a situation not uncommonly encountered in proteins with a high content of helical secondary structure – only triple-resonance NOESY experiments allow an unambiguous extraction of distance information. Very recently, O. Zhang et al. (1996,1997) have developed a similar approach suitable for the assignment of NOEs in unfolded proteins. Since in disordered states the dispersion of backbone ^{15}N and ^{13}C resonances is considerably better than that of the proton resonances, in their pulse sequences interresidual $^{1}H,^{1}H$ NOEs are identified via correlations between heteronuclei of the two amino acid residues involved. Frequency labelling of heteronuclei instead of the source and the target protons requires several coherence transfer steps both before and after the NOE mixing period. For proteins in the native state, however, resonance overlap can usually be removed already by correlating either the source or the target proton spins with one or more heteronuclei belonging to the same scalar coupling network, leading to somewhat simpler pulse sequences. A $^{13}C'$-edited NOESY-H(N)CO experiment which is closely related to one of the experiments considered in this paper has recently been introduced by W. Zhang et al. (1996) for the same purpose.

Methods

The novel pulse sequences described in this paper catenate NOE mixing times with some of the most sensitive triple-resonance techniques. The correlations obtained in each of the experiments are summarized in Fig. 1. As the coherence transfer mechanisms of the scalar correlation elements have previously been analysed in detail, only a brief description is given in the following.

Basically, in triple-resonance NOESY experiments dipolar interactions can be detected for protons which constitute either the origin or the destination of the magnetization transfer via the scalar coupling network. Although the two alternatives are obviously equivalent in the case of 'out-and-back'-type experiments, some practical differences arise, as will be discussed below. NOE connectivities of amide protons can be obtained using the pulse sequences of Fig. 2. The two schemes are based on the constant-time HNCO and the constant-time HN(CO)CA experiments (Grzesiek and Bax, 1992a), respectively. The NOE mixing periods are appended at the end of the sequences, such that not only amide protons are detected during acquisition, but also those protons involved in dipolar interactions with the former. A drawback of this scheme is that protons resonating in the vicinity of the strong water signal cannot be detected or exhibit reduced signal intensities. The problem can, in principle, be circumvented by interchanging the triple-resonance and the NOESY portions as realized in the ^{13}C'-edited NOESY-H(N)CO experiment (W. Zhang et al., 1996). We preferred, however, the HNCO-NOESY variant, because in contrast to a NOESY-HNCO, amide protons and other ^{1}H species can be detected in a single frequency domain. Thus, in 3D versions of the experiments it is possible to separate the NOE cross peaks by ^{13}C' and ^{15}N instead of only ^{13}C' chemical shifts. Furthermore, the NOE correlations – most prone to spectral overlap – are aligned in the

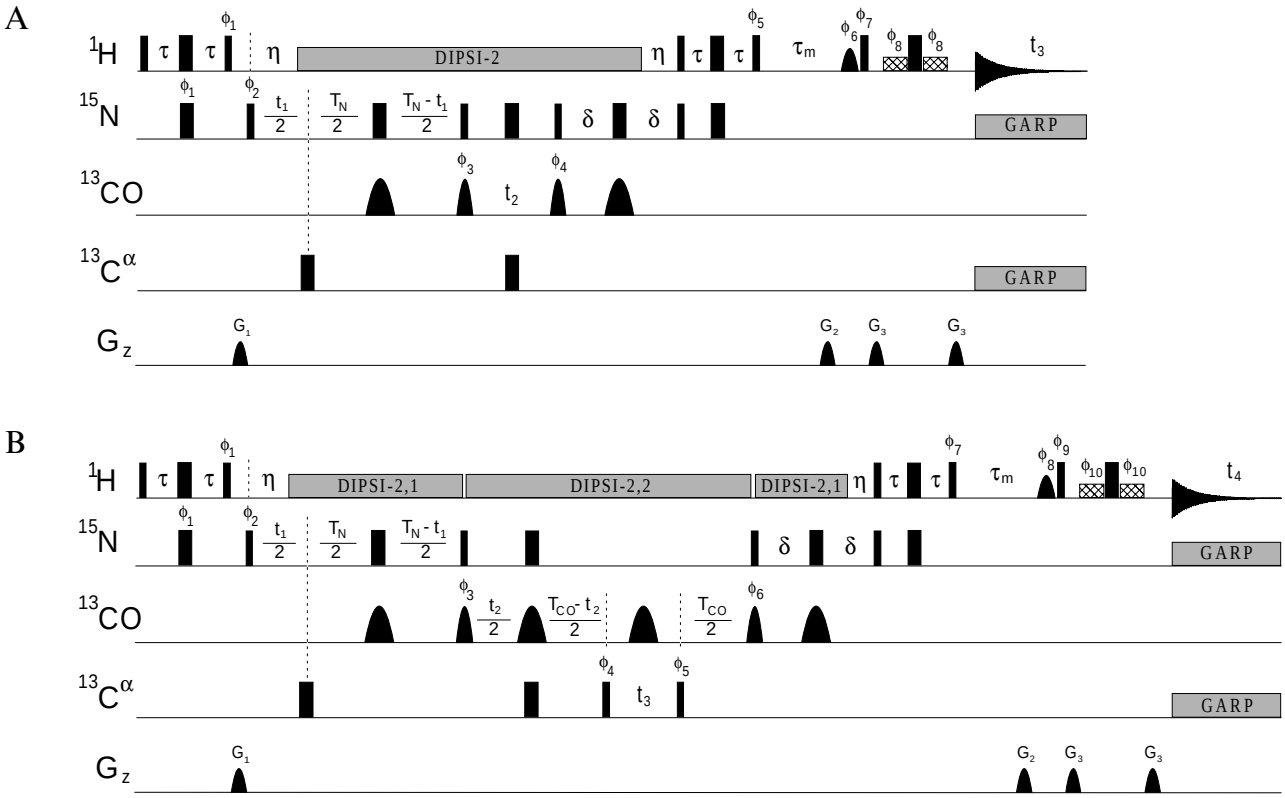

Fig. 2. Pulse sequences of the HNCO-NOESY (A) and the HNCOCA-NOESY (B) experiment. Narrow and wide bars denote rectangular pulses corresponding to flip angles of 90° and 180°, respectively. Pulses on ^{13}CO are centred at 176 ppm while ^{13}C$^{\alpha}$ pulses, excluding the CPD sequences, are applied at 56 ppm in (A) and at 58 ppm in (B). The widths of pulses on α-carbons are adjusted to provide a null in their excitation profile at the carbonyl region. Carbonyl 90° and 180° pulses are sinc-shaped and have durations of 124 μs at 600 MHz and 100 μs at 800 MHz spectrometers. The proton carrier frequency is placed on the water resonance and is switched to the centre of the amide region for DIPSI-2 decoupling (Shaka et al., 1988) with the exception of the second decoupling period in (B), labelled DIPSI-2,2, where the carrier is returned to the H_2O frequency. Cross-hatched rectangles denote 2.5 ms low-power 90° pulses. The water-selective 90° pulses applied at the end of the NOE mixing periods τ_m are Gaussian-shaped and have a duration of 15 ms. GARP-1 decoupling (Shaka et al., 1985) of ^{15}N nuclei is applied with rf field strengths of 0.76 kHz and 0.96 kHz at resonance frequencies of 60.8 MHz and 81.8 MHz, respectively. For carbon GARP decoupling during acquisition, the carrier frequency is positioned at 43 ppm, and the rf field is adjusted to 2.27 kHz at 150.9 MHz and to 2.78 kHz at 201.2 MHz resonance frequencies, adequate to cover the entire aliphatic region. Gradient pulses are sine-bell-shaped. The durations and approximate amplitudes in the centre of G_1, G_2 and G_3 are 1 ms, 10 G cm^{-1}, 2 ms, 15 G cm^{-1}, 0.8 ms, 35 G cm^{-1}. Delay durations and phase cycles are as follows: (A) $\tau = 2.3$ ms, $\eta = 5.4$ ms, $T_N = 28$ ms, $\delta = 14$ ms, $\tau_m = 150$ ms, $\phi_1 = y,-y$, $\phi_2 = 2(x),2(-x)$, $\phi_3 = 8(x),8(-x)$, $\phi_4 = 4(x-55°),4(-x-55°)$, $\phi_5 = y$, $\phi_6 = 8(-x),8(x)$, $\phi_7 = 8(x),8(-x)$, $\phi_8 = -x$, rec. = x,2(–x),x,–x,2(x),–x; and (B) $\tau = 2.3$ ms, $\eta = 5.4$ ms, $T_N = 28$ ms, $T_{CO} = 18$ ms, $\delta = 14$ ms, $\tau_m = 130$ ms, $\phi_1 = y,-y$, $\phi_2 = 2(x),2(-x)$, $\phi_3 = x,-x$, $\phi_4 = 4(x),4(-x)$, $\phi_5 = x+55°$, $\phi_6 = x-65°$, $\phi_7 = y$, $\phi_8 = 4(-x),4(x)$, $\phi_9 = 4(x),4(-x)$, $\phi_{10} = -x$, rec. = 2(x),2(–x). Nonlabelled pulses are applied along the x-axis. Compensation of zero-order Bloch–Siegert phase errors is achieved by empirical adjustment of pulse phases as indicated. Quadrature in the indirectly detected dimensions is obtained by incrementing phases ϕ_2 and ϕ_3 (HNCO-NOESY) and ϕ_2, ϕ_3 and ϕ_4 (HNCOCA-NOESY) in the States-TPPI manner (Marion et al., 1989b).

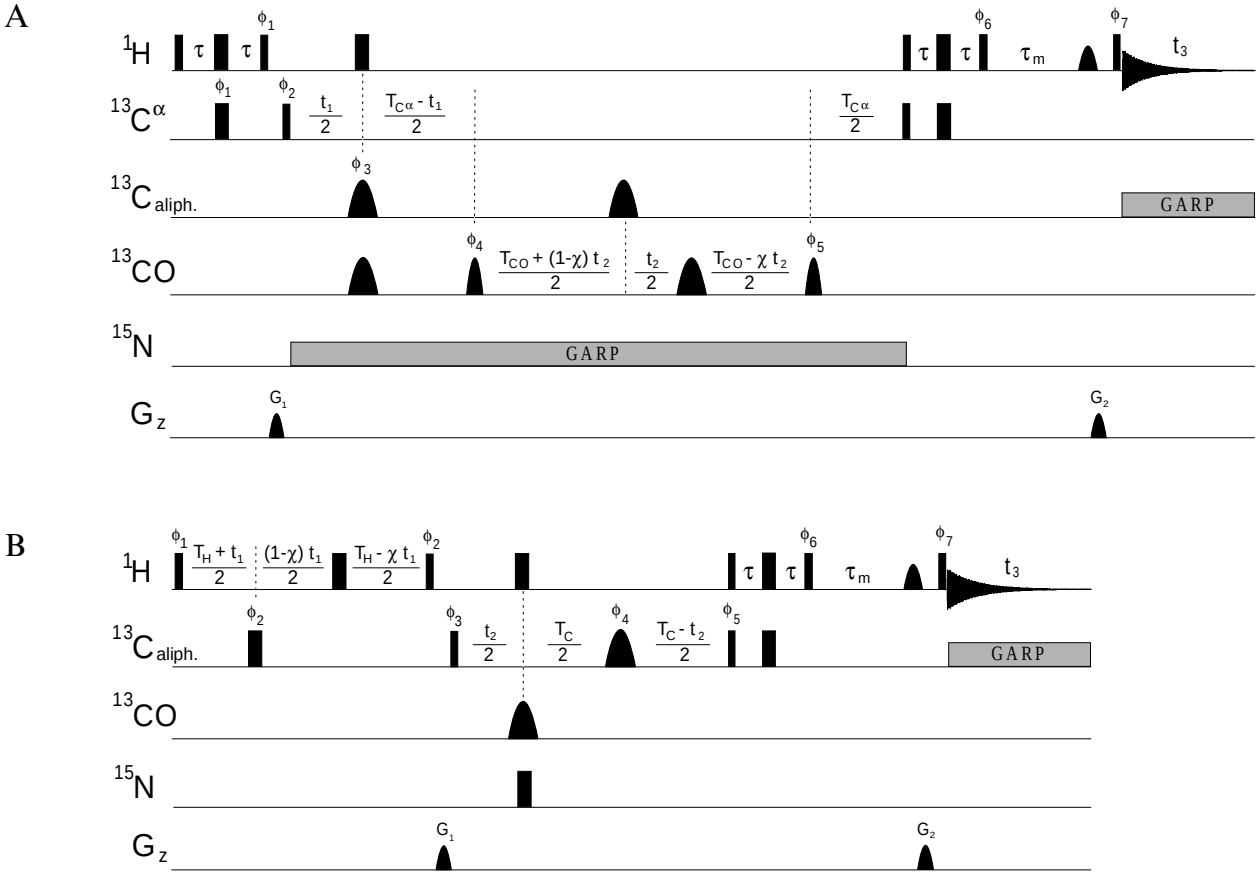

Fig. 3. Experimental schemes for the HCACO-NOESY (A) and the ct-HSQC-NOESY (B) experiments. The phase of pulses is x unless otherwise indicated. All proton pulses are applied with an rf field of 16.3 kHz with the exception of the Gaussian-shaped water-selective 90° pulse at the end of τ_m which has a duration of 15 ms. The ^{1}H carrier frequency is placed on the H_2O resonance (4.75 ppm) throughout the HCACO-NOESY and following the 90° pulse labelled ϕ_2 in the ct-HSQC-NOESY while it is 2.7 ppm during the t_1 evolution time. Pulses on α-carbons are applied at 56 ppm with rf field strengths of 6.25 kHz and 17.1 kHz for 90° and 180° flip angles, respectively. Band-selective refocusing pulses on aliphatic carbons are G3 Gaussian cascades (Emsley and Bodenhausen, 1990) centred at 46 ppm (duration: 300 μs) in the HCACO-NOESY and at 41 ppm (duration: 250 μs) in the ct-HSQC-NOESY. The rf field for all rectangular pulses on aliphatic carbons in (B) is 17.1 kHz. GARP decoupling during acquisition (2.8 kHz rf field) is applied at 41 ppm. Carbonyl 90° and 180° pulses are sinc-shaped and have durations of 100 μs. These pulses are centred at 176 ppm by phase modulation. Gradient durations and strengths are G_1: 1 ms, 10 G cm^{-1} and G_2: 2 ms, 30 G cm^{-1} in both experiments. Delays and phase cycles: (A) $\tau = 1.7$ ms, $T_{C\alpha} = 18$ ms, $T_{CO} = 9.4$ ms, $\tau_m = 100$ ms, $\phi_1 = y,-y$, $\phi_2 = 2(x),2(-x)$, $\phi_3 = 8(x),8(y)$, $\phi_4 = 4(x),4(-x)$, $\phi_5 = x+70°$, $\phi_6 = y$, $\phi_7 = 8(x),8(-x)$, rec. = x,2(–x),x,–x,2(x),–x; and (B) $T_H = 3.5$ ms, $T_C = 27$ ms, $\tau = 1.7$ ms, $\tau_m = 100$ ms, $\phi_1 = 4(x),4(-x)$, $\phi_2 = y,-y$, $\phi_3 = 2(x),2(-x)$, $\phi_4 = 8(x),8(y)$, $\phi_5 = x-21°$, $\phi_6 = y$, $\phi_7 = 8(x),8(-x)$, rec. = x,2(–x),x,–x,2(x),–x. The phases labelled ϕ_5 are adjusted to compensate for the effects of Bloch–Siegert shifts. Phases ϕ_2 (t_1), ϕ_4 (t_2) and ϕ_1 (t_1), ϕ_3 (t_2) are incremented in the States-TPPI manner in (A) and (B), respectively. The factors χ have values of 0.63 in scheme A and 0.34 in scheme B.

directly detected dimension which usually provides the highest resolution. Editing of NOEs to amide protons via the three heteronuclear species of the protein backbone can be achieved with the 4D HNCOCA-NOESY. The coherence transfer between $^{13}C^{\alpha}$ and $^{13}C'$ nuclei is implemented as an HMQC-type element. Evolution of carbonyl chemical shifts takes place during the periods for de- and refocusing of $^{13}C'$ antiphase magnetization with respect to α-carbons in a full-sweep constant-time manner (Madsen and Sørensen, 1992; Van Doren and Zuiderweg, 1994).

Solvent suppression in the 3D HNCO-NOESY and the 4D HNCOCA-NOESY is achieved by the WATERGATE technique (Piotto et al., 1992). Relatively long selective 90° pulses on the H_2O resonance (2.5 ms) were employed to minimize the width of the bleached region in the centre of the spectra. A saturation of fast-exchanging amide protons (Li and Montelione, 1993) was avoided by a 15 ms Gaussian-shaped flip-back pulse (Grzesiek and Bax, 1993a,b; Kay et al., 1994; Stonehouse et al., 1994) applied at the end of the NOE mixing time (Lippens et al., 1995). Here, the fact is exploited that, as a result of radiation damping, the water magnetization has completely returned to the +z-axis at the duration of the mixing periods used (Jahnke and Kessler, 1994; Jahnke et al., 1995; Otting and Liepinsh, 1995).

In analogy to the HNCO-NOESY, NOE effects of α-protons can be detected in an HCACO-NOESY sequence, i.e. the NOE cross peaks are not only correlated with the

heteronucleus directly bound to the source spin, but with the adjacent carbonyl carbon, too. Due to the distinct scalar coupling networks, the respective pulse sequence cannot be derived from the former simply by interchanging ^{15}N and $^{13}C^{\alpha}$ channels. In the original ct-HCACO experiment (Powers et al., 1991), the fixed durations T for the build-up and refocusing of $^{13}C^{\alpha}$ antiphase magnetization with respect to $^{13}C'$ are set to 7 ms in order to optimize the expression $\sin^2[\pi\,{}^1J(C^{\alpha},C')T]\cos^2[\pi\,{}^1J(C^{\alpha},C^{\beta})T]\exp(-2T/T_{2,C^{\alpha}})$. The resolution in the constant-time $^{13}C^{\alpha}$ dimension can be substantially improved while both trigonometric terms have their maximum value by adjusting T to the inverse of $^1J(C^{\alpha},C^{\beta})$ (Palmer et al., 1992). Relaxation during an ≈54 ms period of transverse $^{13}C^{\alpha}$ magnetization can, however, degrade signal intensities considerably. In the pulse sequence shown in Fig. 3A, the $^{13}C^{\alpha}$,$^{13}C'$ polarization transfer steps are replaced by an HMQC-like element with an overall duration of $[^1J(C^{\alpha},C^{\beta})]^{-1}$ (≈27 ms), with the delays for de- and rephasing of transverse $^{13}C^{\alpha}$ magnetization with respect to $^{13}C'$ tuned to $T_{C^{\alpha}}/2 = [2\,{}^1J(C^{\alpha},C')]^{-1}$ (Löhr and Rüterjans, 1995a). Therefore, any loss of detectable magnetization due to the passive $^1J(C^{\alpha},C^{\beta})$ coupling or incomplete evolution of the active $^1J(C^{\alpha},C')$ coupling is avoided while the influence of ^{13}C T_2 relaxation is tolerable.

For comparison of the sensitivity and the chemical shift dispersion in the HCACO-NOESY spectrum, a conventional carbon-resolved NOESY spectrum was

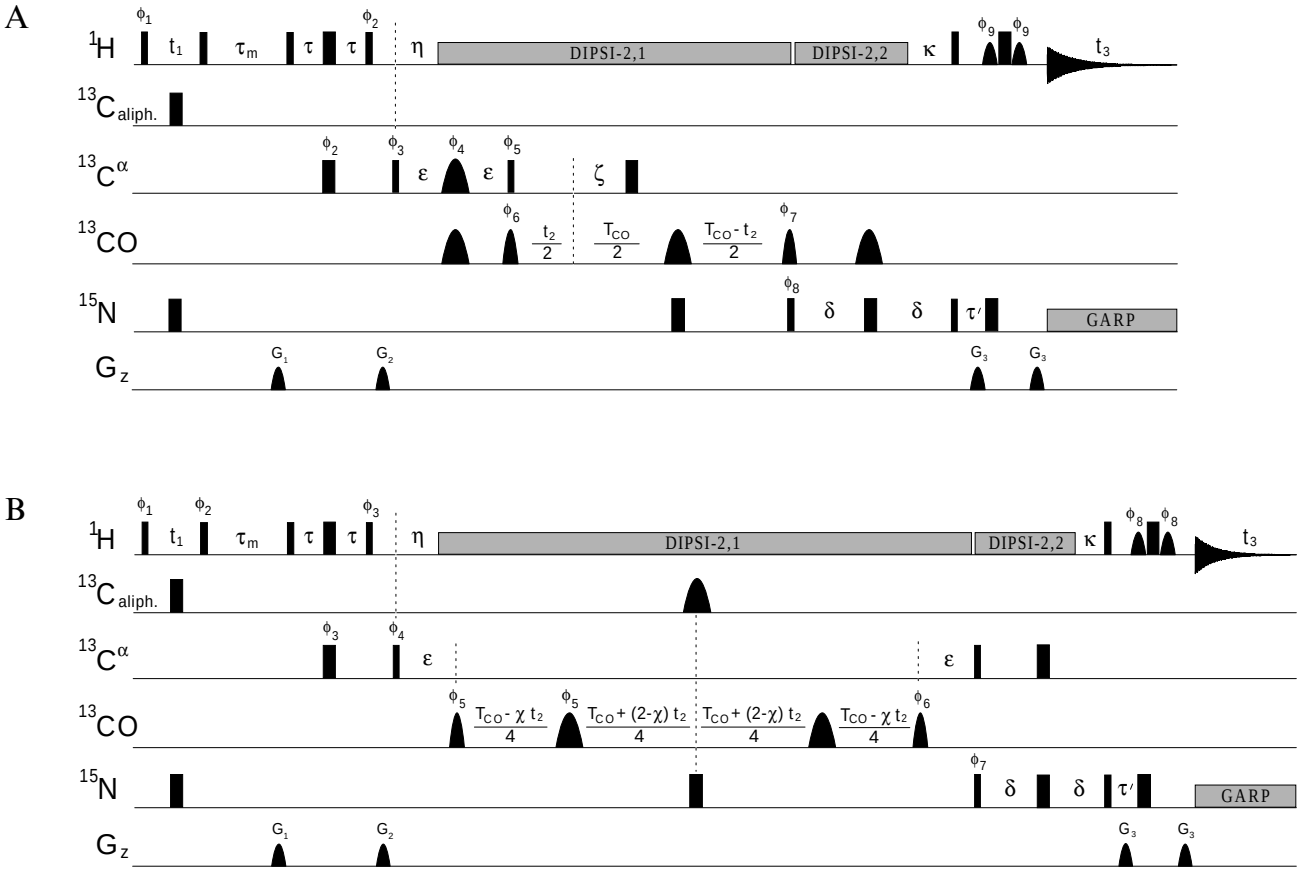

Fig. 4. (A) NOESY-(HCA)CO(N)H sequence and (B) NOESY-(HCA)CO(CAN)H sequence. Pulses on the $^{13}C^{\alpha}$ and $^{13}C'$ channels are centred at 58 and 175.7 ppm, respectively. The power levels for rectangular 90° and 180° $^{13}C^{\alpha}$ pulses are adjusted such that no excitation in the carbonyl region occurs. The inversion pulses in the centre of the t_1 evolution period are applied at 43 ppm with an rf field strength of 17.6 kHz, while the refocusing pulse in the centre of t_2 in the NOESY-(HCA)CO(CAN)H is a 300 μs G3 pulse applied at an offset of 46 ppm. In the NOESY-(HCA)CO(N)H, the 180° $^{13}C^{\alpha}$ pulse labelled ϕ_4 is a G3 pulse with a duration of 1 ms. The width of all sinc-shaped $^{13}C'$ pulses is 124 μs. The proton carrier frequency corresponds to 4.75 ppm throughout the sequences except for the DIPSI-2,2 decoupling periods (4 kHz rf field), where it is switched to 8.5 ppm. Water-selective 90° pulses in the final reverse INEPT part are Gaussian-shaped and have a duration of 2.5 ms. All nitrogen pulses are applied at 121.1 ppm with rf fields of 8 kHz for hard pulses and 0.76 kHz for GARP decoupling. Durations and approximate strengths of pulsed field gradients are G_1: 1 ms, 15 G cm^{-1}; G_2: 1 ms, 15 G cm^{-1}; G_3: 0.8 ms, 35 G cm^{-1} in both sequences. The gradients in the WATERGATE sequence are followed by recovery delays of 200 μs. Further delays are tuned to (A) $\tau_m = 100$ ms, $\tau = 1.7$ ms, $\eta = 3.4$ ms, $\varepsilon = 7.8$ ms, $T_{CO} = 28$ ms, $\zeta = 4.6$ ms, $\delta = 14$ ms, $\kappa = 5.4$ ms, $\tau' = 2.7$ ms; and (B) $\tau_m = 100$ ms, $\tau = 1.7$ ms, $\eta = 3.4$ ms, $\varepsilon = 9$ ms, $T_{CO} = 9.3$ ms, $\delta = 12$ ms, $\kappa = 5.4$ ms, $\tau' = 2.7$ ms. The factor χ has the value 0.5. Phase cycling is as follows: (A) $\phi_1 = 8(x),8(-x)$, $\phi_2 = y,-y$, $\phi_3 = 2(x),2(-x)$, $\phi_4 = 4(x),4(-x)$, $\phi_5 = x{-}30°$, $\phi_6 = 4(x),4(-x)$, $\phi_7 = x{-}58°$, $\phi_8 = 8(x),8(-x)$, $\phi_9 = -x$, rec. = x,2(−x),x,−x,2(x),−x; and (B) $\phi_1 = 8(x),8(-x)$, $\phi_2 = 16(x),16(-x)$, $\phi_3 = y,-y$, $\phi_4 = 2(x),2(-x)$, $\phi_5 = 4(x),4(-x)$, $\phi_6 = x{-}96°$, $\phi_7 = 16(x),16(-x)$, $\phi_8 = -x$, rec. = x,2(−x),x,−x,2(x),2(−x),2(x),−x,x,2(−x),x. Nonlabelled pulses have the phase x. Quadrature in F1 is obtained by TPPI (Marion and Wüthrich, 1983) of the phase ϕ_1 , while the States-TPPI method is applied to ϕ_6 (A) and ϕ_5 (B) for sign discrimination in F2.

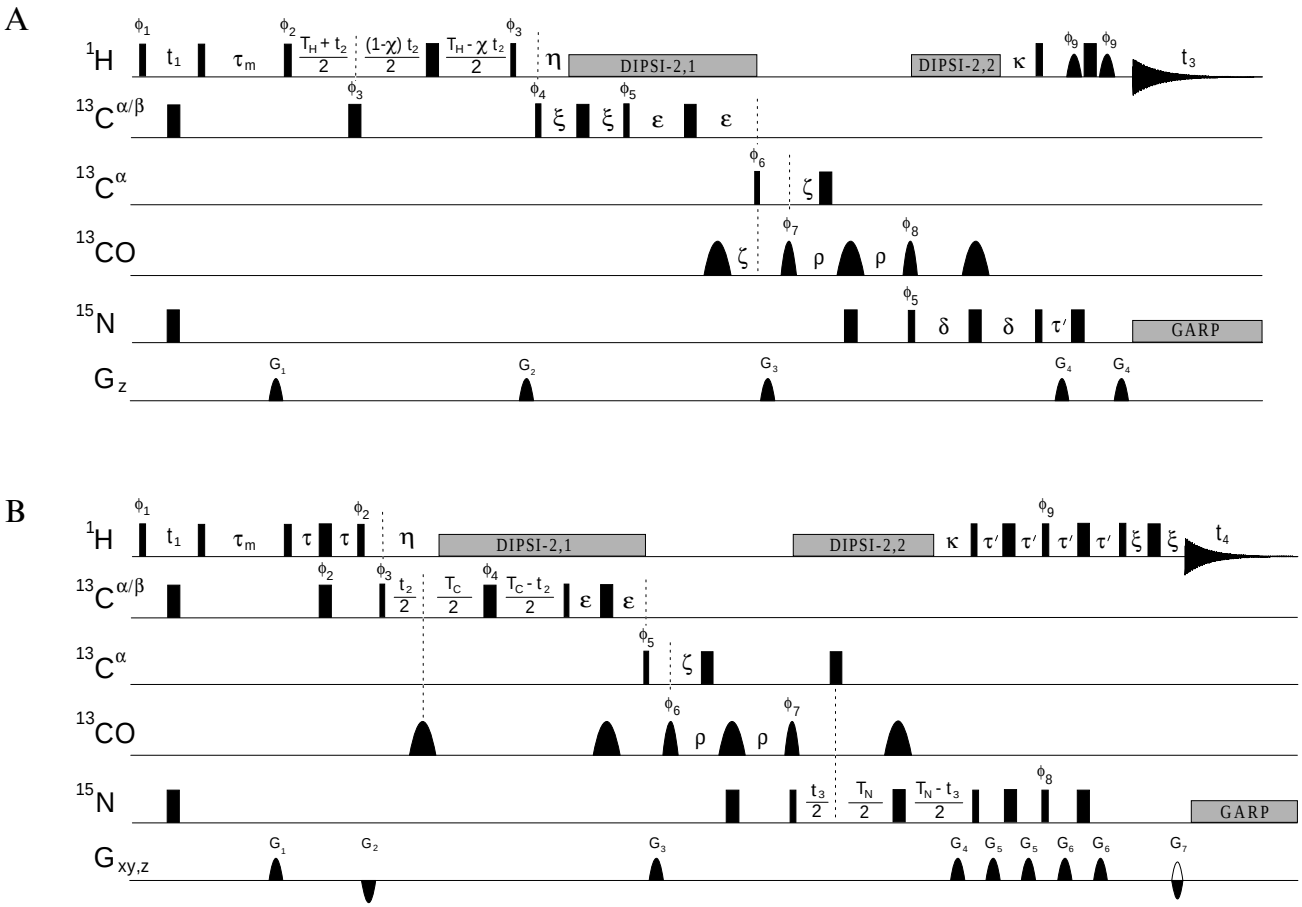

Fig. 5. Pulse schemes of the NOESY-HB(CBCACON)H (A) and the NOESY- CBCA(CO)NH (B) experiment. Nonlabelled pulses are applied along the x-axis. Pulses on $^{13}C^{\alpha/\beta}$, $^{13}C^{\alpha}$ and $^{13}C'$ are centred at 46, 58 and 176 ppm, respectively. Carbonyl pulses have an amplitude profile corresponding to the centre lobe of a sinc function and a duration of 100 μs, irrespective of their flip angle. All the remaining ^{13}C pulses are rectangular. Their widths are adjusted to provide a null in the excitation profile at the carbonyl region, except for the initial inversion pulse which is applied with an rf field of 17.1 kHz. Four different ^{1}H carrier positions are employed in the course of the NOESY-HB(CBCACON)H sequence, i.e. 4.0 ppm (t_1), 2.9 ppm (t_2, DIPSI-2,1), 8.5 ppm (DIPSI-2,2) and 4.75 ppm (reverse INEPT, t_3). The 2 ms water-selective 90° pulses are Gaussian-shaped. In the NOESY-CBCA(CO)NH sequence, the proton carrier frequency is 3.8 ppm up to the first DIPSI-2 decoupling period, then changed to 8.5 ppm for the second DIPSI-2 sequence and finally to the position of the H_2O resonance. The rf field strengths for proton and nitrogen decoupling are 4.2 and 0.95 kHz, respectively. Durations and approximate strengths of sine-bell-shaped pulsed field gradients along z are (A) G_1: 2 ms, 10 G cm^{-1}; G_2: 1 ms, 7.5 G cm^{-1}; G_3: 1 ms, 12.5 G cm^{-1}; G_4: 0.8 ms, 35 G cm^{-1}; and (B): G_1: 2 ms, 10 G cm^{-1}; G_2: 1 ms, –17.5 G cm^{-1}; G_3: 1 ms, 12.5 G cm^{-1}; G_5: 0.5 ms, 4 G cm^{-1}; G_6: 0.5 ms, 5 G cm^{-1}. Gradients G_4 and G_7, used for coherence selection in (B), are applied in the transverse plane and have strengths G_4: 39.5 G cm^{-1} (x), 29.6 G cm^{-1} (y) and G_7: –4 G cm^{-1} (x), –3 G cm^{-1} (y) at a duration of 1 ms. Delay settings and phase cycles are as follows: (A) $\tau_m = 100$ ms, $T_H = 3.5$ ms, $\eta = 1.85$ ms, $\xi = 3.5$ ms, $\varepsilon = 6.9$ ms, $\zeta = 4.6$ ms, $\rho = 13$ ms, $\delta = 14$ ms, $\kappa = 5.4$ ms, $\tau' = 2.7$ ms, $\phi_1 = 8(x),8(-x)$, $\phi_2 = x$, $\phi_3 = y,-y$, $\phi_4 = 2(x),2(-x)$, $\phi_5 = 8(x),8(-x)$, $\phi_6 = x+42°$, $\phi_7 = 4(x),4(-x)$, $\phi_8 = x+50°$, $\phi_9 = -x$, rec. = x,2(–x),x,–x,2(x),–x; and (B) $\tau_m = 120$ ms, $\tau = 1.7$ ms, $\eta = 1.85$ ms, $T_C = 7$ ms, $\varepsilon = 3.8$ ms, $\zeta = 4.6$ ms, $\rho = 13$ ms, $T_N = 28$ ms, $\kappa = 5.4$ ms, $\tau' = 2.5$ ms, $\xi = 1.5$ ms, $\phi_1 = x,-x$, $\phi_2 = 4(y),4(-y)$, $\phi_3 = 2(x),2(-x)$, $\phi_4 = x+9°$, $\phi_5 = x+42°$, $\phi_6 = 4(x),4(-x)$, $\phi_7 = x+50°$, $\phi_8 = y$, $\phi_9 = y$, rec. = x,2(–x),x. The factor χ in the semi-constant-time t_2 evolution time of the NOESY-HB(CBCACON)H has the value 0.36. For every other FID in the NOESY-CBCA(CO)NH experiment, the sign of G_7 together with the phase ϕ_8 is inverted to select the echo and antiecho coherence transfer pathways. Quadrature in F1 is obtained by TPPI applied to ϕ_1 in both experiments, and incrementation of ϕ_2 and ϕ_3 in sequences A and B, respectively, according to the States-TPPI protocol leads to sign discrimination in F2. The phases of 90° or 180° pulses are adjusted to compensate for zero-order Bloch–Siegert phase errors as indicated.

recorded in a constant-time version using the pulse sequence in Fig. 3B. The HCACO-NOESY pulse sequence can be derived from the ct-HSQC-NOESY by inserting a $^{13}C'$ evolution time into the $^{13}C_{aliph}$ constant-time period. Thus, the delay $T_C = [^1J(C^{\alpha},C^{\beta})]^{-1}$ is shared for the chemical shift evolution of α-carbon and carbonyl nuclei in the HCACO-NOESY. The maximum $^{13}C^{\alpha}$ evolution time $T_{C\alpha}$ is determined by the $^{13}C^{\alpha}$,C' one-bond coupling (see above), providing a reasonable resolution in the F1 dimension ($t_{1,max} \approx 18$ ms). The remaining time T_{CO} which can be used for $^{13}C'$ chemical shift evolution is relatively short, such that only a moderate resolution would be obtained in F2, if the incrementation is carried out in a constant-time manner. The resolution can, however, be improved by a factor $1/\chi$ ($= t_{2,max}/T_{CO}$) when the semi-constant-time protocol (Logan et al., 1992; Grzesiek and Bax, 1993c) is applied. In the present implementation, $t_{2,max}$ was prolonged from 9.4 ms (T_{CO}) to 14.8 ms by setting χ to 0.63.

Note that it is not possible to choose arbitrarily long $t_{2,max}$ values because a modulation with the passive $^1J(C^\alpha,C^\beta)$ coupling, scaled down by $1 - \chi(= [(t_{2,max} - T_{CO})/t_{2,max}])$, occurs as a consequence of the $^{13}C^\alpha$,$^{13}C'$ multiple-quantum coherence during T_{CO}. In a similar manner, the transfer time of the initial INEPT step in the ct-HSQC-NOESY was incorporated in the ^1H (t_1) evolution period.

Both the HCACO-NOESY and the ct-HSQC-NOESY experiments were carried out on a protein sample dissolved in D_2O. The remaining HDO signal was suppressed by a single, relatively long selective pulse at the end of the NOE mixing time, followed by the spoiler gradient pulse G_2 (Haase et al., 1985; Doddrell et al., 1986), such that protein resonances nearly degenerate with the solvent could be detected. Nitrogen decoupling should be applied during acquisition, if a sample with H_2O as the solvent is used in order to observe NOE effects between α- and amide protons.

Like the HCACO-NOESY experiment, the NOESY-(HCA)CO(N)H (Fig. 4B) has been designed to record NOE connectivities of α-protons. The basic difference is that the NOE mixing time is placed at the beginning of the sequence and the magnetization is relayed from $^1H^\alpha$ spins 'straight-through' to amide protons of the following residue via one-bond scalar couplings (Boucher et al., 1992). Therefore, two proton dimensions are given, leaving the choice between three heteronuclear species, i.e. $^{13}C^\alpha$, $^{13}C'$ and ^{15}N, for a further dispersion in a 3D version of the experiment. In the variant described here, $^{13}C'$ has been selected, such that the NOESY-(HCA)CO(N)H has two frequency domains in common with the HCACO-NOESY and only one with the ^1H,^{13}C HSQC-NOESY.

As amide protons are detected, the use of H_2O as the solvent is mandatory. Water suppression is easily achieved using the WATERGATE method, and, in contrast to the HNCO-NOESY and the HNCOCA-NOESY, virtually no decrease in signal intensity is associated with the non-uniform excitation profile, because the NOE correlations are sampled in an indirect dimension at F3 positions far from the water resonance. Note that in the pulse sequences of Fig. 4, the final ^{15}N inversion pulse is slightly displaced from the centre of the reverse INEPT delay, as suggested by Simorre et al. (1995), such that more selective pulses on the H_2O resonance can be used while the duration for refocusing of proton antiphase magnetization is fixed at $(2\,^1J_{NH})^{-1} = 2\tau'$.

The triple-resonance portion (Löhr and Rüterjans, 1995b) of the NOESY-(HCA)CO(CAN)H scheme shown in Fig. 4B can be regarded as a concatenation of the HCACO with an HCANNH (Montelione and Wagner, 1990; Kay et al., 1991; Boucher et al., 1992) sequence. Intra- and interresidual connectivities are obtained via $^1J(C^\alpha,N)$ and $^2J(C^\alpha,N)$ couplings, respectively. Instead of recording $^{13}C^\alpha$ chemical shifts, however, the one-bond C^α,C' coupling is exploited to correlate amide with carbonyl chemical shifts. Although the HN(CA)CO experiment (Clubb et al., 1992) essentially provides the same type of information for backbone resonance assignments, only the sequence employed here is suitable for the detection of NOEs involving $^1H^\alpha$ spins.

In the NOESY-(HCA)CO(N)H, the influence of the

TABLE 1
ACQUISITION PARAMETERS FOR THE HETERONUCLEAR EDITED NOESY EXPERIMENTS

Experiment	Mixing time (ms)	Nucleus				Time domain data points[a]				Spectral width (Hz)				Acquisition time (ms)				No. of scans per FID	Total exp. time (h)
		F1	F2	F3	F4	t_1	t_2	t_3	t_4	F1	F2	F3	F4	t_1	t_2	t_3	t_4		
HNCO-NOESY	150	^{15}N	$^{13}C'$	^1H		23	78	768		1429	1825	8993		15.4	42.5	85.4		16	39
HNCOCA-NOESY	130	^{15}N	$^{13}C'$	$^{13}C^a$	^1H	10	18	20	640	1538	1958	3623	9191	6.5	8.7	5.5	69.7	8	72.5
HCACO-NOESY	100	$^{13}C^\alpha$	$^{13}C'$	^1H		68	36	768		5000	2404	9766		13.6	14.8	78.7		16	48
ct-HSQC-NOESY	100	^1H	^{13}C	^1H		50	60	768		4902	4026	9766		10.0	14.8	78.7		16	58
NOESY-(HCA)CO(N)H	100	^1H	$^{13}C'$	$^1H^N$		224[b]	42	1024		6098	1506	8993		18.3	27.2	113.9		16	89
NOESY-(HCA)-CO(CAN)H	100	^1H	$^{13}C'$	$^1H^N$		216[b]	28	1024		6098	1506	8993		17.7	18.0	113.9		32	109
NOESY-HB-(CBCACON)H	100	^1H	$^1H^{\beta\,c}$	$^1H^N$		200[b]	36	768		7143	3676	9124		14.0	9.7	84.2		16	67.5
NOESY-CBCA(CO)NH	120	^1H	$^{13}C^{\alpha/\beta}$	^{15}N	$^1H^N$	52[b]	22	8	640	6579	7507	1314	9124	5.3	2.8	4.0	70.2	8	88

[a] Complex points unless otherwise marked.
[b] Real points.
[c] $^1H^\alpha$ for Gly.

passive $^1J(C^\alpha,C^\beta)$ coupling during the C^α,C' polarization transfer step is minimized using a C^α-selective refocusing pulse in the centre of the delay 2ε. An optimization of the coherence transfer efficiency in the NOESY-(HCA)-CO(CAN)H is achieved in a similar manner as described above for the HCACO-NOESY by employing a C^α,C' HMQC element with an overall duration tuned to $[^1J(C^\alpha,C^\beta)]^{-1}$. Again, the ^{13}C' evolution is of the semi-constant-time type, this time expanding $t_{2,max}$ from 9.3 ms to 18.6 ms ($\chi = 0.5$).

The pulse sequences depicted in Fig. 5 are multiple relayed triple-resonance NOESY experiments based on the CBCA(CO)NH scheme (Grzesiek and Bax, 1992b). Hence, the magnetization transfer pathway of the NOESY-(HCA)CO(N)H is extended by a C,C-COSY step, allowing the detection of NOE effects in which β-protons are the target spins. In the 3D NOESY-HB(CBCACON)H experiment (Fig. 5A), ^{1}H chemical shifts are sampled in a semi-constant-time manner immediately following the NOE mixing time. Thus, one obtains 'homonuclear' spectra in which the F1/F2 NOESY planes are separated by the $^1H^N$ resonance frequencies of the following amino acid residue. The adjustment of the period 2ε to $[2\,^1J(C^\alpha,C^\beta)]^{-1}$ leads to a selection of $^1H^\beta$ magnetization in t_2. The transfer $C^\beta \rightarrow C^\alpha \rightarrow C'$ is optimized while for all but glycine spin systems the pathway $C^\alpha \rightarrow C^\alpha \rightarrow C'$ is cancelled, neglecting variations in the size of the $^1J(C^\alpha,C^\beta)$ coupling constants. In contrast, NOEs involving β- as well as α-protons are detected in the NOESY-CBCA(CO)NH sequence (Fig. 5B), where 2ε is set to approximately $[4\,^1J(C^\alpha,C^\beta)]^{-1}$. A further difference is that the ^{1}H (t_2) time domain has been replaced by a ^{13}C constant-time evolution period. Finally, an additional heteronuclear dimension has been introduced, aiming at an improved signal dispersion. Recording of ^{15}N chemical shifts was preferred here over a ^{13}C'-edited version because this choice enables the sensitivity enhancement method (Cavanagh and Rance, 1990; Palmer et al., 1991) to be applied. The sensitivity enhancement scheme is combined with gradient coherence selection (Kay et al., 1992b; Schleucher et al., 1994) through gradients G_4 and G_7. Imperfections of the ^{1}H 180° pulses which might result in phase errors in the acquisition domain are eliminated by the gradient pairs G_5 and G_6.

Experimental

Two different samples of uniformly ^{13}C/^{15}N-labelled *Desulfovibrio vulgaris* flavodoxin were employed in the NMR experiments described in the previous section. A 1.5 mM sample dissolved in 99.9% D_2O was used to obtain the HCACO-NOESY and the ct-HSQC-NOESY data sets while a sample containing only 5% D_2O was required for the remaining experiments. The protein concentration of the latter sample was 1.4 mM. Both samples contained 10 mM potassium phosphate and trace amounts of NaN_3 in order to prevent bacterial growth. The pH was 7.0 in H_2O solution and 6.8 in D_2O solution (uncorrected for isotope effects). For all experiments the temperature setting was 300 K.

The following spectra were recorded on a Bruker DMX 800 spectrometer: HNCOCA-NOESY, HCACO-NOESY, ct-HSQC-NOESY, NOESY-HB(CBCACON)H and NOESY-CBCA(CO)NH. The HNCO-NOESY, NOESY-(HCA)CO(N)H and NOESY-(HCA)CO(CAN)H experiments were carried out on a Bruker DMX 600 spectrometer. Both spectrometers were equipped with actively shielded three-axes gradient probes, i.e. a 5 mm $^1H\{^{13}C, ^{15}N\}$ triple resonance and a 5 mm $^1H\{^{13}C,^{31}P,^{15}N\}$ quadruple resonance probe at 600 and 800 MHz proton frequencies, respectively.

Acquisition parameters for each of the data sets are listed in Table 1. It should be noted that in the HCACO-NOESY the carbon carrier was positioned in the $^{13}C^\alpha$ region during the ^{13}C' evolution time because frequency jumps within the period $T_{C\alpha}$ would have resulted in a loss of transmitter phase coherence on our spectrometer. Therefore, using a spectral width of 11.95 ppm, signals are folded 10 times in t_2 with the centre corresponding to an offset of 175.5 ppm. Alternatively, a fourth channel could have been used for pulses on carbonyl spins. Details concerning carrier positions, delay duration and pulse widths and phases in the individual experiments are given in the legends of Figs. 2–5. In addition, a standard 3D NOESY-$^1H\{^{15}N\}$HMQC spectrum was acquired according to Zuiderweg and Fesik (1989) on a Bruker AMX 600 spectrometer without gradient equipment, using a 3.5 mM sample of ^{15}N-labelled flavodoxin. The NOE mixing time was set to 150 ms. Acquisition times were 17.6, 15.4 and 101.4 ms in the t_1 (^{1}H), t_2 (^{15}N) and t_3 ($^1H^N$) domains, respectively. The data collection for the NOESY-HMQC required 64 h, recording eight transients per FID.

Processing of 3D spectra was performed with the Bruker software (XWIN-NMR 1.1), whereas the FELIX 1.1 program (Hare Research Inc.) was used for the two 4D data sets. In indirectly detected, non- (semi-) constant-time dimensions, the initial delay was adjusted such that a 180° or a 360° linear phase correction was required after Fourier transformation. Time domain data were extended by 10–25% using linear prediction in t_1 and t_2 of 3D experiments. In the 4D HNCOCA-NOESY and the 4D NOESY-CBCA(CO)NH, the number of data points was doubled in each of the two constant-time dimensions by mirror-image linear prediction. Prior to Fourier transformation, all time domain data were multiplied by a squared-cosine function. Elimination of the solvent line by convolution of the FIDs was only applied to experiments in which amide protons are detected exclusively, but not in the HNCO-NOESY, the HNCOCA-NOESY, the HCACO-NOESY or the ct-HSQC-NOESY.

Results and Discussion

The proposed triple-resonance NOESY experiments have been applied to the flavodoxin from *Desulfovibrio vulgaris* in its oxidized state. It consists of a single 147 amino acid polypeptide chain and a noncovalently bound FMN molecule (molecular mass: 16.3 kDa). Proton and nitrogen resonance assignments for this protein were reported by us and by others (Knauf et al., 1993; Stockman et al., 1993). The solution structure has been determined recently by NMR using NOE-derived distance restraints and ϕ dihedral angle restrictions (Knauf et al., 1996). Like other flavodoxins, it consists of a central five-stranded parallel β-sheet which is surrounded by two helices on each side. Carbon resonance assignments have been obtained and will be published elsewhere. Despite the comparatively good chemical shift dispersion observed for flavodoxin, a simultaneous degeneracy of proton and heteronuclear chemical shifts in two CH or two NH groups is encountered several times. As a consequence, NOEs that originate from these protons cannot be differentiated in conventional 3D heteronuclear edited NOESY spectra. The introduction of a fourth dimension in $^{13}C/^{13}C$ (Clore et al., 1991; Zuiderweg et al., 1991), $^{13}C/^{15}N$ (Kay et al., 1990a) or $^{15}N/^{15}N$ (Grzesiek et al., 1995; Venters et al., 1995) separated NOESY experiments does allow a more reliable identification of the second proton involved in the dipolar interaction, but the ambiguity concerning the source proton remains. In triple-resonance NOESY experiments, protons are correlated with backbone spins via two or more one-bond scalar couplings, thus spreading out the cross peaks that overlap in the $^{1}H^{N}/^{15}N$ or $^{1}H^{\alpha}/^{13}C^{\alpha}$ planes, for instance.

The general appearance of triple-resonance NOESY spectra is illustrated in Fig. 6. In the amide region of the HNCO-NOESY and HNCOCA-NOESY spectra, strong cross peaks represent the direct correlations corresponding to diagonal peaks in a 3D ^{15}N separated NOESY. Dipolar interactions of the amide protons lead to extra cross peaks lined up along the acquisition domain at the same heteronuclear chemical shifts as the direct correlations. Thus, the information provided by triple-resonance experiments about scalar connectivities within the protein backbone is retained, at the same time allowing the identification of short interproton distances. In the versions of the HNCO-NOESY and HNCOCA-NOESY pulse sequences employed here, the detection of α-proton resonances in the proximity of the H_2O signal is hampered by the nonuniform excitation profile of the WATERGATE solvent suppression scheme. However, as can be recognized from Fig. 6, the bleached region could be restricted to approximately ± 0.25 ppm around the proton carrier position, such that the majority of $^{1}H^{\alpha}$ resonances in flavodoxin were observed.

While compared to HNCO and HNCOCA experiments the benefit of the respective triple-resonance NOESY spectra lies in the additional information which can be exploited for secondary and tertiary structure determination, the improved signal dispersion makes them a valuable supplement to the ^{15}N separated NOESY. In the case

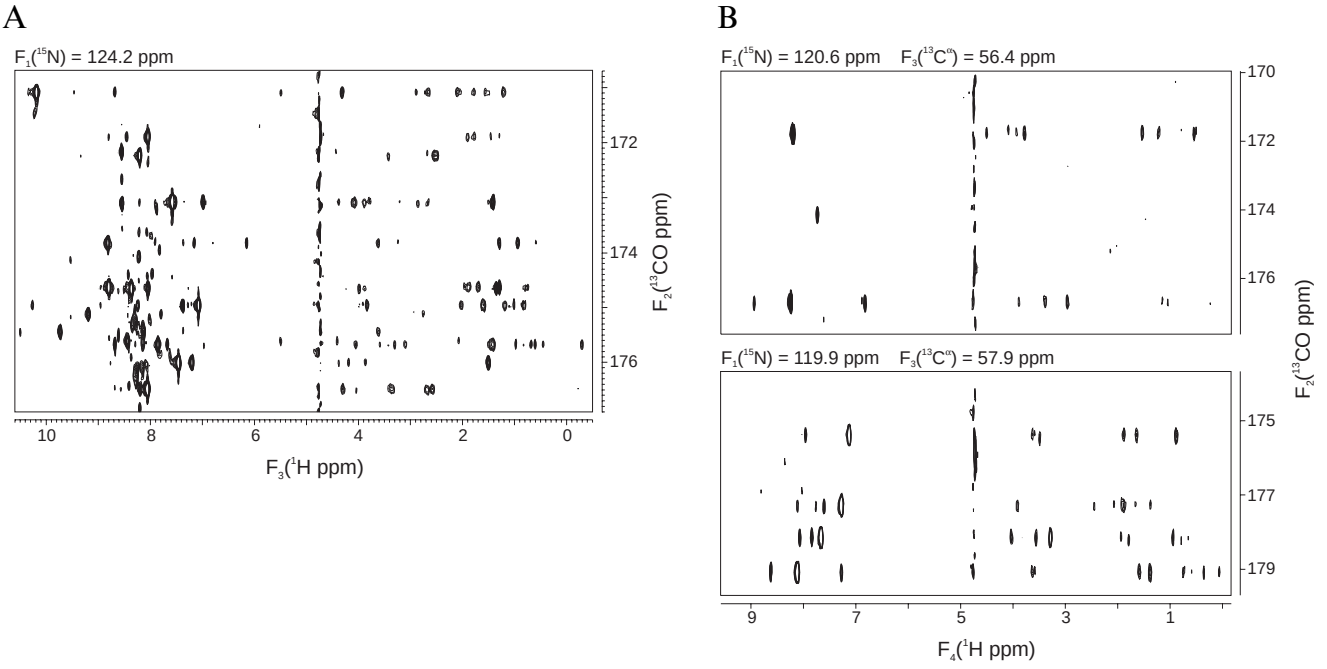

Fig. 6. Representative $^{1}H/^{13}C'$ slices from 3D HNCO-NOESY (A) and 4D HNCOCA-NOESY (B) spectra of *Desulfovibrio vulgaris* flavodoxin. NOE correlations of amide protons are aligned along F3 and F4, respectively, at the F2 carbonyl resonance positions of the preceding amino acid residues.

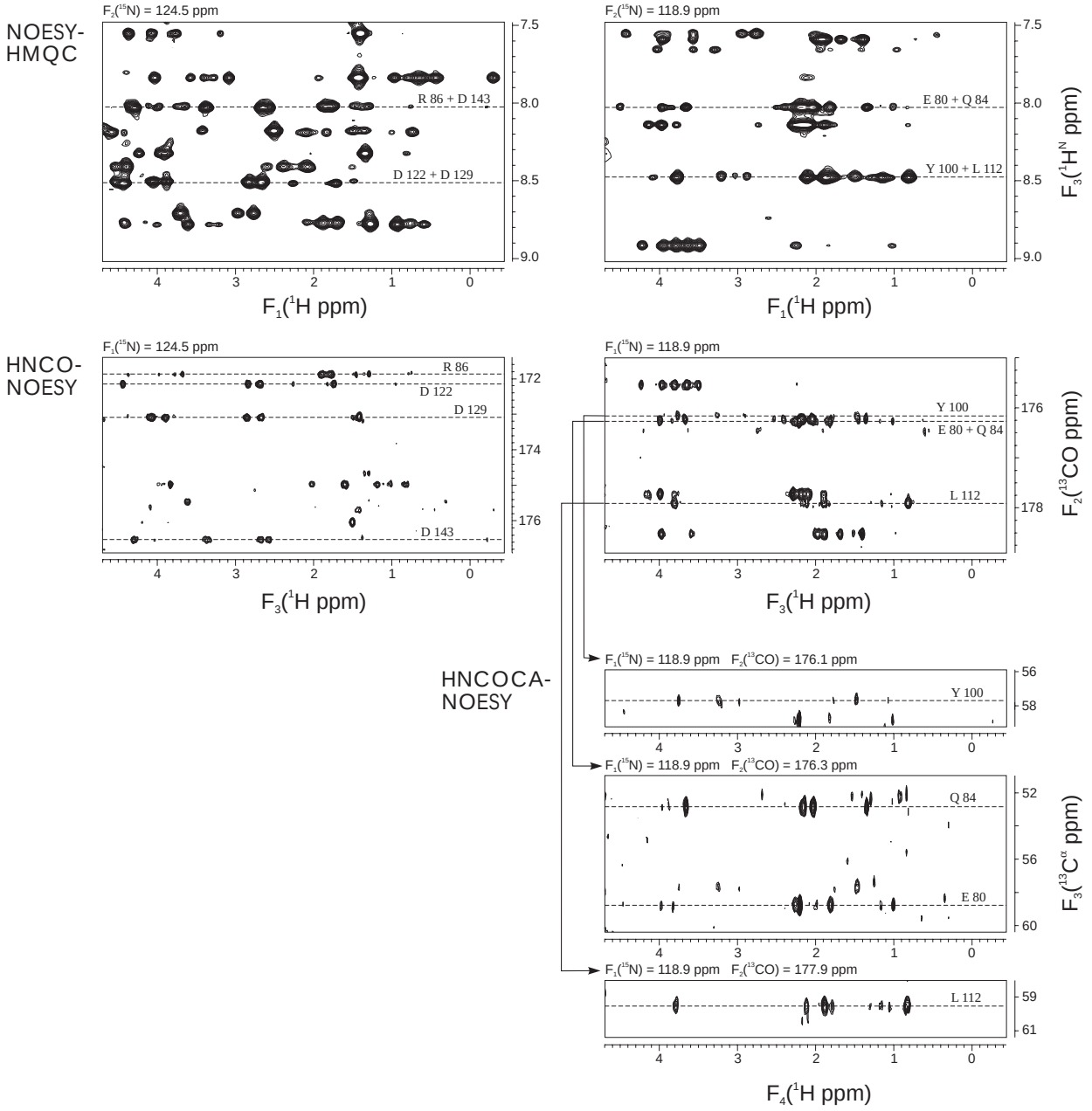

Fig. 7. High-field regions of ^{15}N, $^{15}N/^{13}C'$ and $^{15}N/^{13}C'/^{13}C^{\alpha}$ resolved NOESY spectra of flavodoxin. Dashed lines mark the position of NOE cross peaks to the amide protons of residues Arg^{86}, Asp^{122}, Asp^{129} and Asp^{143} (left side) and of Glu^{80}, Gln^{84}, Tyr^{100} and Leu^{112} (right side). In order to facilitate the comparison of the spectra, the NOESY-HMQC plots are rotated such that the acquisition domain is represented by the vertical axis. The degeneracy of $^{1}H^{N}/^{15}N$ chemical shifts within the pairs Arg^{86}/Asp^{143} and Asp^{122}/Asp^{129} can be resolved via $^{13}C'$ chemical shifts in the HNCO-NOESY, while for the pairs Glu^{80}/Gln^{84} and Tyr^{100}/Leu^{112} a complete separation can only be accomplished with the help of the HNCOCA-NOESY. The arrows indicate the carbonyl frequencies in the HNCO-NOESY at which the F3/F4 slices from the HNCOCA-NOESY are taken.

of flavodoxin, there are four residue pairs, i.e. Glu^{80}/Gln^{84}, Asp^{122}/Asp^{129}, Arg^{86}/Asp^{143} and Tyr^{100}/Leu^{112}, possessing identical resonance frequencies of amide protons attached to ^{15}N nuclei with likewise nearly identical chemical shifts. Since, furthermore, the ^{15}N chemical shifts of Arg^{86}, Asp^{122}, Asp^{129} and Asp^{143} are close together, as are those of the remaining four residues, they appear in only two F1/F3 planes of the NOESY-HMQC spectrum. These slices are shown at the top of Fig. 7. For the pairs Arg^{86}/Asp^{143} and Asp^{122}/Asp^{129}, the ambiguity in the assignment of NOEs involving the amide protons is easily resolved with the help of the HNCO-NOESY experiment. In the F2/F3 slice that corresponds to the same ^{15}N position as the respective slice in the NOESY-HMQC, the cross peaks are well separated due to the different $^{13}C'$ chemical shifts. A more unfavourable situation is encountered for the

residues in the second slice selected from the ^{15}N-edited NOESY. Here, the assignment is complicated by the fact that not only are the $^{1}H^{N}$ and ^{15}N resonances of Glu^{80} and Gln^{84} degenerate but also the ^{13}C' resonances of the sequentially preceding residues. In addition, the resonance frequency of the carbonyl bound to the amide of Tyr^{100} differs by only 0.1 ppm, leading to an even more severe overlap in the 3D HNCO-NOESY. The problem can be solved by correlating the $^{1}H^{N}/^{15}N(i)$ resonances with $^{13}C'(i-1)$ as well as $^{13}C^{\alpha}(i-1)$ chemical shifts in a 4D HNCOCA-NOESY experiment. As demonstrated in Fig. 7, the dispersion provided by the α-carbon dimension removes the overlap present in both the NOESY-HMQC and the HNCO-NOESY.

A direct comparison of the sensitivity between the NOESY-HMQC and the triple-resonance NOESY experiments is not possible because of the different experimental conditions (spectrometer hardware, sample concentrations) chosen for recording the spectra in this study. Clearly, the signal-to-noise ratio is considerably higher in the NOESY-HMQC as in the HNCO-NOESY, which can be mainly attributed to the higher protein concentration of the sample (3.5 mM versus 1.4 mM) and the longer measuring time (64 h versus 39 h). It can, however, be stated that the vast majority of NOE connectivities found in the NOESY-HMQC could also be identified in the HNCO-NOESY.

As mentioned above, signal overlap occurs for *D. vulgaris* flavodoxin not only in the $^{1}H/^{15}N$ region of heteronuclear correlation spectra but also in the aliphatic region. First, it will be discussed how ambiguous NOE cross peaks of degenerate α-protons can be assigned more reliably. A straightforward adaptation of the HNCO-NOESY for this purpose is the HCACO-NOESY experiment. The mixing due to cross relaxation takes place after the 'out-and-back' scalar correlation scheme, such that the NOE connectivities are sampled in the acquisition domain. In order to assess the gain in the dispersion of $^{1}H^{\alpha}$ NOEs offered by the HCACO-NOESY pulse sequence, a 3D ^{13}C-resolved ct-HSQC-NOESY with a mixing period of equal duration was recorded at 800 MHz. Strips from ct-HSQC-NOESY $^{1}H/^{1}H$ planes are compared to the corresponding sections of the HCACO-NOESY spectrum in Fig. 8. The α-protons of residues Glu^{79} and Glu^{110} as well as those of Leu^{46} and Glu^{48} have identical resonance frequencies. Although this kind of overlap is usually resolved in the ^{13}C dimension of a 3D HSQC-NOESY spectrum, in the examples chosen, an assignment of NOEs is prevented by the additional degeneracy of the directly bound carbons. Again, the correlation to carbonyl chemical shifts yields the desired separation of diagonal and cross peaks. In the $^{13}C'/^{1}H$ slices of the HCACO-NOESY, dipolar interactions of pairwise degenerate α-CH groups appear at two different positions along the F2 dimension.

Only minor differences in the signal-to-noise ratios were found between the ct-HSQC-NOESY and the HCACO-NOESY spectra. This observation is not unexpected since the duration of fixed delays is virtually identical in the two sequences, leading to an equal attenuation of signal intensity due to transverse relaxation. It is clear that a better sensitivity would be obtained in the non-constant-time version of the HSQC-NOESY, but it should be excluded here that the comparison of the spectral disper-

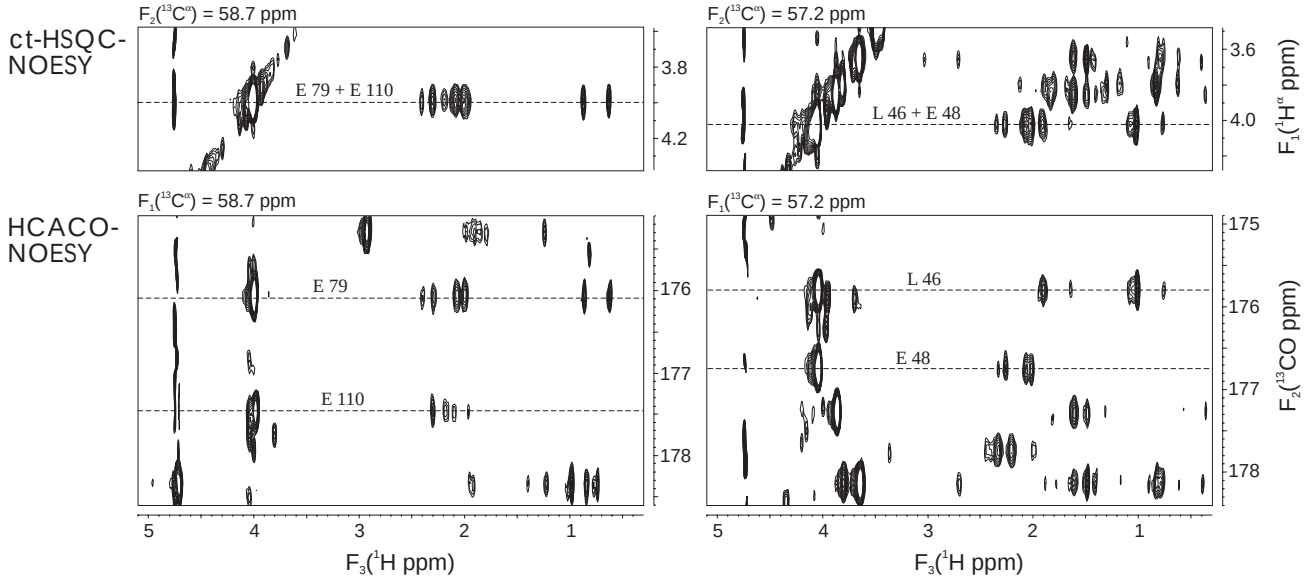

Fig. 8. Separation of NOEs from $C^{\alpha}H$ groups with identical ^{1}H and ^{13}C chemical shifts. F1/F3 and F2/F3 slices, respectively, from the ct-HSQC-NOESY spectrum and the HCACO-NOESY spectrum, both recorded at 800 MHz, using a sample of *D. vulgaris* flavodoxin in 99.9% D_2O are shown. The cross sections at the left (right) are taken at the common $^{13}C^{\alpha}$ chemical shift of Glu^{79} and Glu^{110} (Leu^{46} and Glu^{48}).

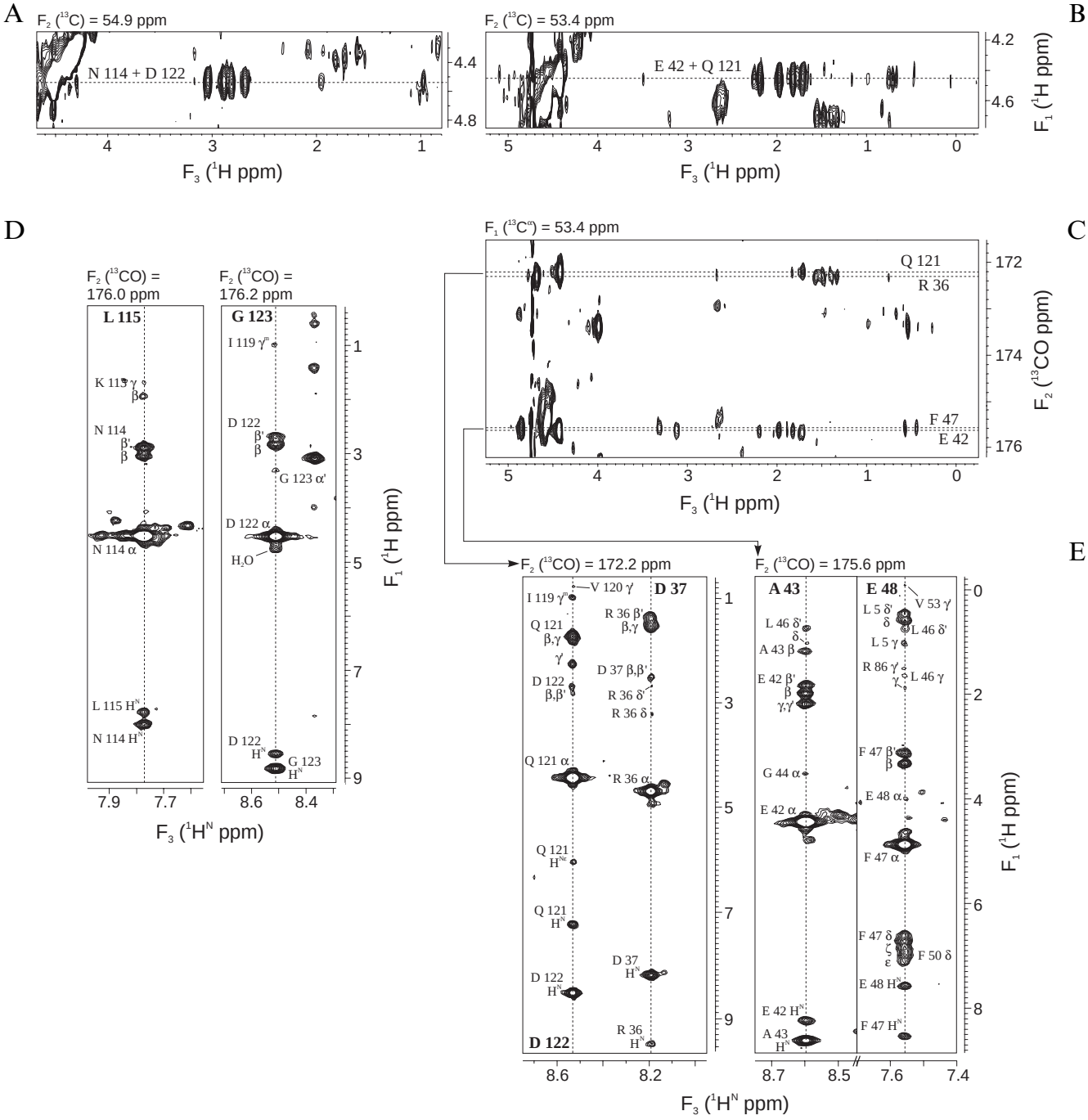

Fig. 9. Use of the NOESY-(HCA)CO(N)H experiment for the unambiguous assignment of NOEs involving α-protons. Strips from ct-HSQC-NOESY (A,B), HCACO-NOESY (C) and NOESY-(HCA)CO(N)H (D,E) spectra of flavodoxin, recorded at 800 MHz (HSQC-NOESY, HCACO-NOESY) and 600 MHz (NOESY-(HCA)CO(N)H), respectively, are shown. Dashed lines indicate the positions of the degenerate $^{1}H^{\alpha}$ resonances of Asn^{114}/Asp^{122} (A) and Glu^{42}/Gln^{121} (B), the carbonyl resonance frequencies of Arg^{36}, Glu^{42}, Phe^{47} and Gln^{121} (C) and the $^{1}H^{N}$ chemical shifts of the residues sequentially following the α-protons to which NOE effects are observed (D,E). Individual assignments of cross peaks are given in the F1/F3 strips of the NOESY-(HCA)CO(N)H.

sions disfavours the HSQC-NOESY simply because of a $^{13}C^{\alpha}$ signal broadening by a modulation with the passive $^{1}J(C^{\alpha},C^{\beta})$ coupling. The $^{13}C^{\alpha}$,$^{13}C'$ coherence transfer step in the HCACO-NOESY is not associated with a loss of sensitivity as a complete build-up and refocusing of $^{13}C^{\alpha}$ antiphase magnetization with respect to $^{13}C'$ can be achieved, neglecting the relatively small variation in $^{1}J(C^{\alpha},C')$ coupling constants. Thus, the main contribution to a potentially decreased sensitivity can be expected from the effect of rf inhomogeneity caused by the additional two 90° and two 180° ^{13}C pulses in the HCACO-NOESY sequence.

The NOESY-(HCA)CO(N)H experiment represents an alternative to the HCACO-NOESY in cases where $^{13}C'$ resonance frequencies coincide and/or NOEs to exchangeable protons should be observed. Since the transfer via cross relaxation takes place at the beginning of the sequence and exclusively amide protons are recorded during acquisition, solvent suppression does not interfere with the detection of NOE interactions of α-protons. After submission of our manuscript, a pulse sequence which is closely related to the NOESY-(HCA)CO(N)H experiment has been published by Zhang and Gmeiner (1996). Two examples for the removal of ambiguity in a conventional ^{13}C-edited NOESY spectrum are illustrated in Fig. 9. The simultaneous degeneracy of the $^1H^\alpha$ and $^{13}C^\alpha$ resonances of residues Asn[114] and Asp[122] leads to spectral overlap in the 3D ct-HSQC-NOESY spectrum (Fig. 9A) of flavodoxin. In contrast, NOEs involving the α-protons of these amino acids can easily be distinguished in F1/F3 strips of the NOESY-(HCA)CO(N)H due to different amide proton chemical shifts of the respective sequentially following residues. Note that the $^{13}C'$ resonance frequencies differ by only 0.2 ppm so that partial overlap remains in the HCACO-NOESY spectrum (not shown), although the complete degeneracy is eliminated.

Not surprisingly, it is now possible to observe NOE connectivities to amide resonances, whereas for the HSQC-NOESY and the HCACO-NOESY a sample dissolved in D_2O was chosen in order to retain all $^1H^\alpha$ signals irrespective of their offset from the solvent resonance. It is, however, worth mentioning that in the NOESY-(HCA)CO-(N)H, a cross peak to the H_2O resonance is detected at the F3 position of Gly[123] $^1H^N$ (Fig. 9D). We tentatively assign this cross peak to a dipolar interaction between Asp[122] $^1H^\alpha$ and an internal water molecule that is part of the hydrogen bond network between the fourth and the fifth strands of the parallel β-sheet in *D. vulgaris* flavodoxin. Previously, the localization of a water molecule at this site was based on strong negative NOEs to the amide protons of Cys[90] and Gly[123] and the $^1H^\beta$ and $^1H^{s\gamma}$ resonances of Cys[90] (Knauf et al., 1996), indicative of a relatively long residence time. We were, however, unable to identify the NOE to the Asp[122] α-proton in the NMR experiments performed thus far. It is, furthermore, remarkable that several weak NOE effects involving aliphatic protons could be observed in the strips from the NOESY-(HCA)CO(N)H (Figs. 9D and E) that were present neither in the HCACO-NOESY nor in the ct-HSQC-NOESY spectra recorded with an identical mixing time. This indicates that the NOESY-(HCA)CO(N)H is a fairly sensitive experiment.

Pairwise degeneracy of $^1H^\alpha/^{13}C^\alpha$ resonances was also found for residues Glu[42] and Gln[121] of flavodoxin (see Fig. 9B). Again, the HCACO-NOESY spectrum was not suitable for a separation of the respective NOE cross peaks, even though in this case the $^{13}C'$ chemical shifts differ by more than 3 ppm. However, accidental $^{13}C^\alpha/^{13}C'$ overlap between Glu[42] and Phe[47] as well as between Gln[121] and Arg[36] (Fig. 9C) prevented an unambiguous assignment of NOE cross peaks although not of HCACO autopeaks. Note that, due to the different $^1H^\alpha$ chemical shifts, the correlations of Arg[36] and Phe[47] do not give rise to any complications in the ct-HSQC-NOESY. As demonstrated

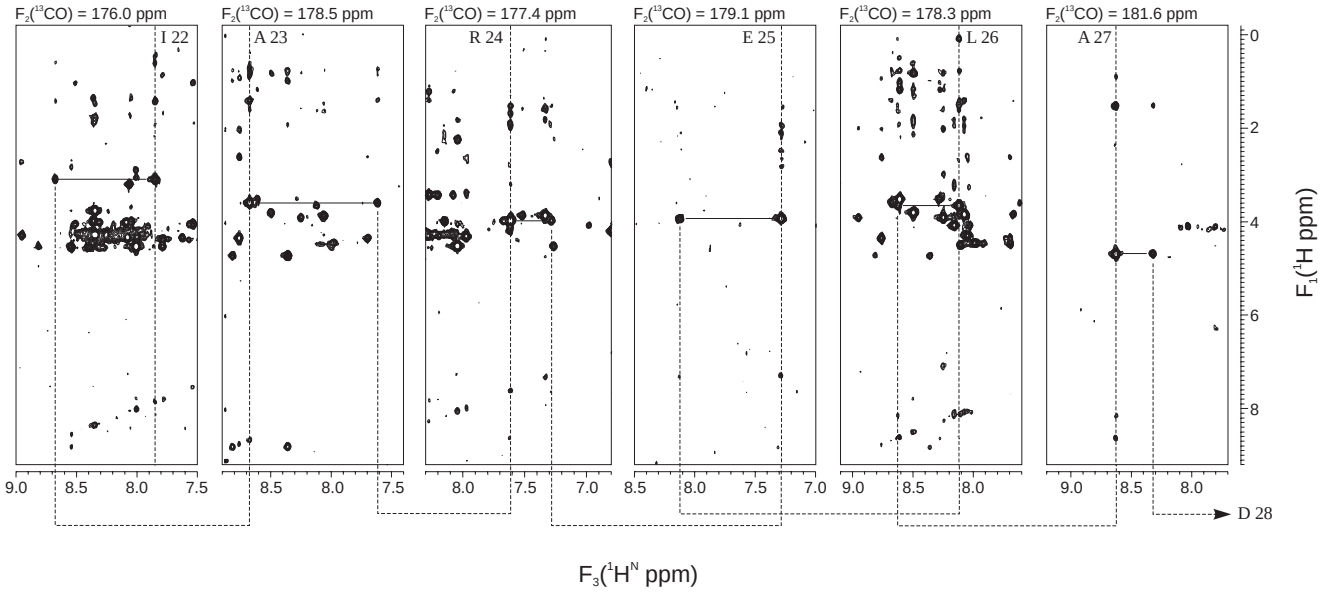

Fig. 10. Sequential assignment of residues Ile[22]–Ala[27] from the first α-helix of *D. vulgaris* flavodoxin in a 3D NOESY-(HCA)CO(CAN)H spectrum. The F1/F3 strips are taken at the $^{13}C'$ chemical shifts of the amino acids specified at the top. Solid lines connect intraresidual $^1H^\alpha(i)/^1H^N(i)$ with interresidual $^1H^\alpha(i)/^1H^N(i+1)$ cross peaks. Signals on the vertical dashed line are NOE correlations to the $^1H^\alpha(i)$ spins. Sequential connectivities can be found via common $^1H^N$ chemical shifts, as indicated.

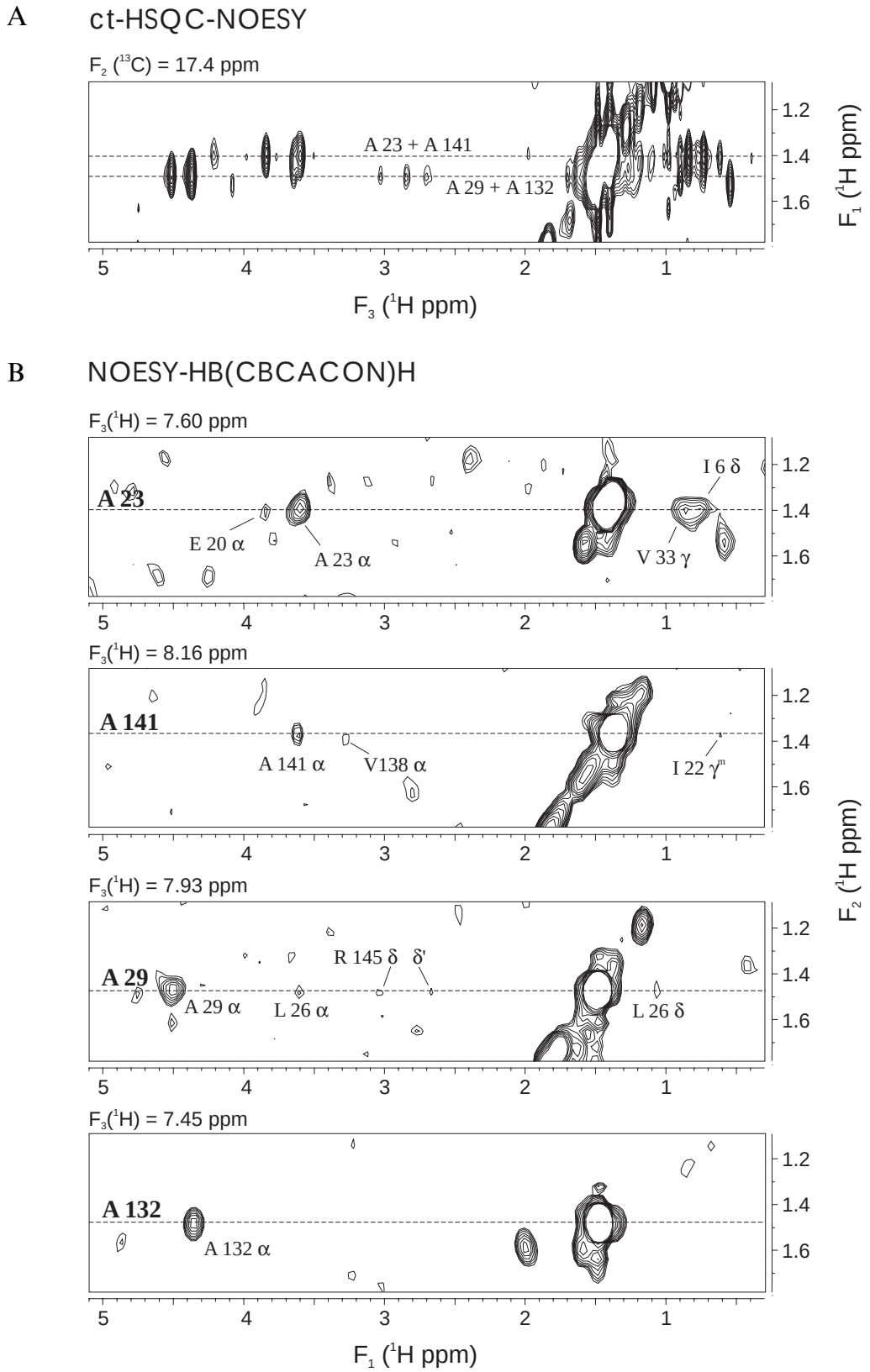

Fig. 11. (A) Expansion from an F1/F3 slice of a ct-HSQC-NOESY spectrum; (B) expansions from F1/F2 slices of a NOESY-HB(CBCACON)H spectrum showing NOE correlations for the β-protons of four alanine residues of flavodoxin. Both data sets were recorded at 800 MHz using a mixing time of 100 ms. The ct-HSQC-NOESY plane is taken at the common $^{13}C^{\beta}$ chemical shifts of Ala^{23}, Ala^{29}, Ala^{132} and Ala^{141}, while the four cross sections through the NOESY-HB(CBCACON)H are at the $^{1}H^{N}$ resonance positions of the respective sequentially following residues. Assignments for the NOE cross peaks are given in the NOESY-HB(CBCACON)H slices.

in Fig. 9E, the identification of NOE interactions for each of the four α-protons is easily achieved by exploiting the dispersion of amide protons in the NOESY-(HCA)CO-(N)H experiment.

The NOESY-(HCA)CO(CAN)H experiment is complementary to the NOESY-(HCA)CO(N)H to the extent that magnetization which resides on α-protons after the NOE transfer is relayed not only to the sequentially following but mainly to the intraresidual amide proton. It correlates $^{1}H^{\alpha}(i)$ chemical shifts along with those of the dipolar interacting protons with $^{13}C'(i)$ and $^{1}H^{N}(i,i+1)$ resonances. Therefore, as shown in Fig. 10, information is provided which permits a sequential walk through the protein backbone. Pairs of cross peaks at common F1 positions identify two neighbouring amide protons in F1/F3 slices of the NOESY-(HCA)CO(CAN)H spectrum. At the same $^{1}H^{N}$ chemical shift as the weaker (i.e. interresidual) cross peak, one has to look for an intraresidual correlation at another $^{13}C'$ position. Here, the next sequential connectivity can be traced, as indicated by the horizontal lines in Fig. 10, and so on. NOEs involving the respective α-protons are lined up along the F1 domain. While scalar correlations were present in the NOESY-(HCA)CO-(CAN)H spectrum of flavodoxin for all but the three proline residues, NOE cross peaks were primarily found at the intraresidual $^{1}H^{N}$ (F3) positions. The reason for the reduced signal-to-noise ratio of the interresidual counterparts is the comparatively inefficient polarization transfer

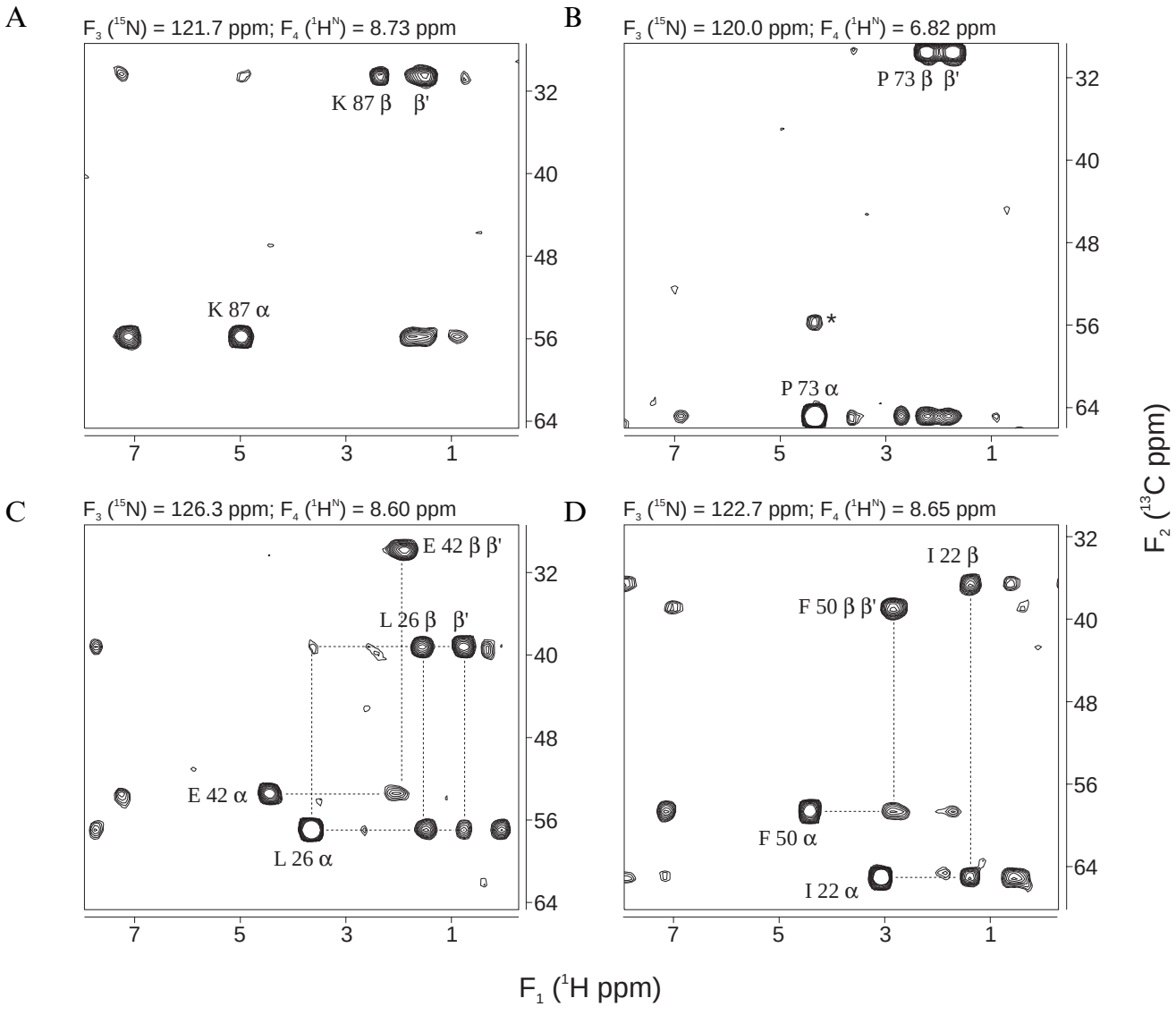

Fig. 12. Application of the 4D NOESY-CBCA(CO)NH experiment to flavodoxin. Cross sections at the ^{15}N (F3) and $^{1}H^{N}$ (F4) positions of Val^{88} (A), Leu^{74} (B), Ala^{27}/Ala^{43} (C) and Ala^{23}/Asp^{51} (D) are shown. The asterisk in (B) marks a cross peak which has its highest intensity in a neighbouring slice. Assignments are only given for $^{1}H^{\alpha}/^{13}C^{\alpha}$ and $^{1}H^{\beta}/^{13}C^{\beta}$ cross peaks. NOE correlations of the respective α- and β-protons are aligned along F1. Dashed lines in (C) and (D) indicate the $d_{\alpha\beta}$ connectivities that allow the identification of ^{13}C resonances belonging to the same residue.

via the $^2J(C^\alpha,N)$ coupling in the presence of the larger passive $^1J(C^\alpha,N)$ coupling. However, the NOE information arising from these signals is redundant and only useful in the case of ambiguity in discovering the $^1H^\alpha(i)/^1H^N(i)$ to $^1H^\alpha(i)/^1H^N(i+1)$ connectivity. It should be noted that this experiment is not useful when triple-resonance methods usually providing this sequential connectivity fail because of fast transverse relaxation encountered in larger proteins, but some additional structural information can be collected if the transfer efficiency is adequate.

Finally, we turn to the application of triple-resonance NOESY experiments for the assignment of NOEs involving side-chain protons. Amino acid types can often be recognized on the basis of characteristic $^1H^\beta$ and $^{13}C^\beta$ chemical shifts. On the other hand, it might therefore not always be straightforward to distinguish cross peaks from different residues of the same type in conventional carbon-resolved NOESY spectra. In the NOESY-HB(CBCACON)H experiment, the dispersion is improved by replacing the ^{13}C by a $^1H^N$ dimension. In more detail, ^1H to $^1H^\beta$ NOE correlations are separated via the amide proton chemical shifts of the sequentially following residues. Figure 11 illustrates the gain in resolution for the example of four alanine residues of flavodoxin. As the β-carbons of Ala^{23}, Ala^{29}, Ala^{132} and Ala^{141} all resonate within 0.3 ppm and the β-proton resonances of Ala^{23} and Ala^{141} as well as those of Ala^{29} and Ala^{132} are virtually degenerate, there is some ambiguity in the respective region of the ct-HSQC-NOESY spectrum. The overlap has been completely removed in the F1/F2 slices of the NOESY-HB(CBCACON)H due to the different chemical shifts of the amide protons to which the $^1H^\beta$ spins are correlated via ^1J scalar couplings. Thus, it is now possible to identify the individual NOEs for each of the four alanine β-protons, among which there are several structurally relevant long-range interactions.

However, one drawback of the NOESY-HB(CBCACON)H, which is also obvious from Fig. 11, should be mentioned. Although strong diagonal peaks, corresponding to the signals in an HB(CBCACON)H, were found for all residues of flavodoxin not followed by a proline, the signal-to-noise ratio was rather poor for most NOE cross peaks, as is obvious from Fig. 11 (the level spacing factor used in all plots of Figs. 7–12 is $2^{1/3}$). The sensitivity of the NOESY-HB(CBCACON)H sequence can be somewhat increased by adjusting the delay ε to ≈3.5 ms instead of 6.9 ms, resulting in a NOESY-HBHA(CBCACON)H experiment. In this version, the influence of transverse $^{13}C^\alpha$ relaxation would be diminished at the expense of a slightly reduced transfer efficiency. The intention in the variant described here was to select β-protons in the F2 dimension. This is in contrast to the NOESY-CBCA(CO)NH experiment, where the respective delay was adjusted to enable NOEs to both α- and β-protons to be detected. As a further modification in the latter sequence, the resonance frequencies of the α- and β-protons themselves are not recorded in t_2, but rather those of the directly bound carbons, such that no diagonal peaks occur. In order to attain the highest possible dispersion of signals, a fourth dimension was introduced. The loss of sensitivity by a factor of $2^{1/2}$, usually associated with the increased dimensionality, is avoided by applying the sensitivity enhancement scheme in the final reverse INEPT step. A disadvantage of sampling carbon instead of proton chemical shifts in t_2 is that, even if stereospecific assignments for β-methylene protons are available, a distinction of their individual NOE effects is no longer possible.

Figure 12 depicts representative F1/F2 planes from a 4D NOESY-CBCA(CO)NH spectrum. In parts A and B, connectivities for a single residue of flavodoxin can be found. The strong peaks are equivalent to what would be obtained in a 4D version of the HBHACBCA(CO)NH experiment (Grzesiek and Bax, 1993a–c; Szyperski et al., 1994), i.e. the sequential correlation of backbone resonances along with residue type information provided by $^1H^\beta/^{13}C^\beta$ chemical shifts. In addition, NOE peaks lined up along F1 at the positions of the α- and β-carbons yield distance information for the directly attached protons. Owing to an almost complete coincidence of amide ^1H and ^{15}N resonances in the amino acids sequentially following Ile^{22} and Phe^{50} (Fig. 12C) as well as Leu^{26} and Glu^{42} (Fig. 12D), the correlations of the α- and β-protons of the residue pairs appear in only one F1/F2 slice in each case. Although not leading to spectral overlap, some ambiguity might arise as it is not a priori clear which nuclei belong to the same spin system. However, in the NOESY-CBCA(CO)NH this problem can be overcome by means of the intraresidual $d_{\alpha\beta}$ NOEs, which only contain more or less trivial distance information but clearly identify the $^1H^\alpha/^{13}C^\alpha$, $^1H^\beta/^{13}C^\beta$ cross peak pairs of the individual residues. As demonstrated by Zhang et al. (1997), NOE connectivities involving side-chain protons beyond the β-position can be established in related triple-resonance NOESY experiments, using a CC-TOCSY instead of a CC-COSY transfer.

Conclusions

It has been shown that editing of $^1H,^1H$ NOESY spectra is not restricted to the directly bound heteronuclei. Recording of triple-resonance NOESY spectra increases the information that can be obtained in a given instrument time in cases where the duration of the measurement is determined by the desired resolution or phase cycling. None of the pulse sequences described here require major changes in the experimental set-up used for the triple-resonance methods from which they are derived. As could be demonstrated, overlap due to a pairwise degeneracy of $^1H/^{15}N$ or $^1H/^{13}C$ resonances, which in

principle cannot be resolved in conventional heteronuclear edited NOESY spectra, is removed by scalar correlations to further nuclei of the protein backbone.

The price to be paid is a loss in signal intensity compared to the pure triple-resonance spectra, caused by longitudinal relaxation during the NOE mixing time. Although this loss is not negligible, we found it to be tolerable for the sample concentrations and magnetic field strengths used in this study, as all scalar correlations expected in each of the experiments were still present. Thus, the application of triple-resonance NOESY experiments can reduce the number of spectra needed to determine solution structures of proteins, while at the same time circumventing difficulties with ambiguous NOE assignments.

Acknowledgements

The authors are grateful to Prof. Stephen G. Mayhew (Department of Biochemistry, University College Dublin) for continuous support with the expression and labelling of the *D. vulgaris* flavodoxin and to Dr. Andrea Hrovat and Markus Blümel for their help with the sample preparations. We thank Dr. Lewis E. Kay for providing his manuscript about related work (Zhang et al., 1997) prior to publication. This work was supported by the Deutsche Forschungsgemeinschaft under Grant Ru 145/11-2.

References

Boucher, W., Laue, E.D., Campbell-Burk, S. and Domaille, P.J. (1992) *J. Am. Chem. Soc.*, **114**, 2262–2264.

Cavanagh, J. and Rance, M. (1990) *J. Magn. Reson.*, **88**, 72–85.

Clore, G.M., Kay, L.E. and Gronenborn, A.M. (1991) *Biochemistry*, **30**, 12–18.

Clowes, R.T., Boucher, W., Hardman, C.H., Domaille, P.J. and Laue, E.D. (1993) *J. Biomol. NMR*, **3**, 349–354.

Clubb, R.T., Thanabal, V. and Wagner, G. (1992) *J. Magn. Reson.*, **97**, 213–217.

Doddrell, D.M., Galloway, G.J., Brooks, W.M., Field, J., Bulsing, J.M., Irving, M.G. and Baddeley, H. (1986) *J. Magn. Reson.*, **70**, 176–180.

Emsley, L. and Bodenhausen, G. (1990) *Chem. Phys. Lett.*, **165**, 469–476.

Grzesiek, S. and Bax, A. (1992a) *J. Magn. Reson.*, **96**, 432–440.

Grzesiek, S. and Bax, A. (1992b) *J. Am. Chem. Soc.*, **114**, 6291–6293.

Grzesiek, S., Anglister, J. and Bax, A. (1993) *J. Magn. Reson.*, **B101**, 114–119.

Grzesiek, S. and Bax, A. (1993a) *J. Am. Chem. Soc.*, **115**, 12593–12594.

Grzesiek, S. and Bax, A. (1993b) *J. Biomol. NMR*, **3**, 627–638.

Grzesiek, S. and Bax, A. (1993c) *J. Biomol. NMR*, **3**, 185–204.

Grzesiek, S., Wingfield, P., Stahl, S., Kaufman, J.D. and Bax, A. (1995) *J. Am. Chem. Soc.*, **117**, 9594–9595.

Haase, A., Frahm, J., Haenicke, W. and Matthei, D. (1985) *Phys. Med. Biol.*, **30**, 341–344.

Ikura, M., Kay, L.E. and Bax, A. (1990) *Biochemistry*, **29**, 4659–4667.

Jahnke, W. and Kessler, H. (1994) *J. Biomol. NMR*, **4**, 735–740.

Jahnke, W., Baur, M., Gemmecker, G. and Kessler, H. (1995) *J. Magn. Reson.*, **B106**, 86–88.

Kay, L.E., Clore, G.M., Bax, A. and Gronenborn, A.M. (1990a) *Science*, **249**, 411–414.

Kay, L.E., Ikura, M., Tschudin, R. and Bax, A. (1990b) *J. Magn. Reson.*, **89**, 496–514.

Kay, L.E., Ikura, M. and Bax, A. (1991) *J. Magn. Reson.*, **91**, 84–92.

Kay, L.E., Ikura, M., Grey, A.A. and Muhandiram, D.R. (1992a) *J. Magn. Reson.*, **99**, 652–659.

Kay, L.E., Keifer, P. and Saarinen, T. (1992b) *J. Am. Chem. Soc.*, **114**, 10663–10665.

Kay, L.E., Xu, G.Y. and Yamazaki, T. (1994) *J. Magn. Reson.*, **A109**, 129–133.

Knauf, M., Löhr, F., Curley, G.P., O'Farrell, P., Mayhew, S.G., Müller, F. and Rüterjans, H. (1993) *Eur. J. Biochem.*, **213**, 167–184.

Knauf, M., Löhr, F., Blümel, M., Mayhew, S.G. and Rüterjans, H. (1996) *Eur. J. Biochem.*, **238**, 423–434.

Li, Y.-C. and Montelione, G.T. (1993) *J. Magn. Reson.*, **B101**, 315–319.

Lippens, G., Dhalluin, C. and Wieruszeski, J.-M. (1995) *J. Biomol. NMR*, **5**, 327–331.

Logan, T.M., Olejniczak, E.T., Xu, R.X. and Fesik, S.W. (1992) *FEBS Lett.*, **314**, 413–418.

Logan, T.M., Olejniczak, E.T., Xu, R.X. and Fesik, S.W. (1993) *J. Biomol. NMR*, **3**, 225–231.

Löhr, F. and Rüterjans, H. (1995a) *J. Magn. Reson.*, **B109**, 80–87.

Löhr, F. and Rüterjans, H. (1995b) *J. Biomol. NMR*, **6**, 189–197.

Lyons, B.A. and Montelione, G.T. (1993) *J. Magn. Reson.*, **B101**, 206–209.

Madsen, J.C. and Sørensen, O.W. (1992) *J. Magn. Reson.*, **100**, 431–436.

Marion, D. and Wüthrich, K. (1983) *Biochem. Biophys. Res. Commun.*, **113**, 967–974.

Marion, D., Driscoll, P.C., Kay, L.E., Wingfield, P.T., Bax, A., Gronenborn, A.M. and Clore, G.M. (1989a) *Biochemistry*, **28**, 6150–6156.

Marion, D., Ikura, M., Tschudin, R. and Bax, A. (1989b) *J. Magn. Reson.*, **85**, 393–399.

Montelione, G.T. and Wagner, G. (1990) *J. Magn. Reson.*, **87**, 183–188.

Montelione, G.T., Lyons, B.A., Emerson, S.D. and Tashiro, M. (1992) *J. Am. Chem. Soc.*, **114**, 10974–10975.

Otting, G. and Liepinsh, E. (1995) *J. Biomol. NMR*, **5**, 420–426.

Palmer III, A.G., Cavanagh, J., Wright, P.E. and Rance, M. (1991) *J. Magn. Reson.*, **93**, 151–170.

Palmer III, A.G., Fairbrother, W.J., Cavanagh, J., Wright, P.E. and Rance, M. (1992) *J. Biomol. NMR*, **2**, 103–108.

Piotto, M., Saudek, V. and Sklenár, V. (1992) *J. Biomol. NMR*, **2**, 661–665.

Powers, R., Gronenborn, A.M., Clore, G.M. and Bax, A. (1991) *J. Magn. Reson.*, **94**, 209–213.

Schleucher, J., Schwendinger, M., Sattler, M., Schmidt, P., Schedletzky, O., Glaser, S.J., Sørensen, O.W. and Griesinger, C. (1994) *J. Biomol. NMR*, **4**, 301–306.

Shaka, A.J., Barker, P.B. and Freeman, R. (1985) *J. Magn. Reson.*, **64**, 547–552.

Shaka, A.J., Lee, C.J. and Pines, A. (1988) *J. Magn. Reson.*, **77**, 274–293.

Simorre, J.-P., Zimmermann, G.R., Pardi, A. and Farmer II, B.T. (1995) *J. Biomol. NMR*, **5**, 427–432.

Stockman, B.J., Euvrad, A., Kloosterman, D.A., Scahill, T.A. and Swenson, R.P. (1993) *J. Biomol. NMR*, **3**, 133–149.

Stonehouse, J., Shaw, G.L., Keeler, J. and Laue, E.D. (1994) *J. Magn. Reson.*, **A107**, 178–184.

Szyperski, T., Pellechia, M. and Wüthrich, K. (1994) *J. Magn. Reson.*, **B105**, 188–191.

Van Doren, S.R. and Zuiderweg, E.R.P. (1994) *J. Magn. Reson.*, **B105**, 193–198.

Venters, R.A., Metzler, W.J., Spicer, L.D., Mueller, L. and Farmer II, B.T. (1995) *J. Am. Chem. Soc.*, **117**, 9592–9593.

Wishart, D.S. and Sykes, B.D. (1994) *J. Biomol. NMR*, **4**, 171–180.

Wüthrich, K. (1986) *NMR of Proteins and Nucleic Acids*, Wiley, New York, NY, U.S.A.

Zhang, O., Kay, L.E. and Forman-Kay, J.D. (1996) *XVIIth International Conference on Magnetic Resonance in Biological Systems*, August 18–23, 1996, Keystone, Colorado, U.S.A., poster MP 88.

Zhang, O., Forman-Kay, J.D., Shortle, D. and Kay, L.E. (1997) *J. Biomol. NMR*, **9**, 181–200.

Zhang, W. and Gmeiner, W.H. (1996) *J. Biomol. NMR*, **8**, 357–359.

Zhang, W., Smithgall, T.E. and Gmeiner, W.H. (1996) *J. Magn. Reson.*, **B111**, 305–309.

Zuiderweg, E.R.P. and Fesik, S.W. (1989) *Biochemistry*, **28**, 2387–2391.

Zuiderweg, E.R.P., Petros, A.M., Fesik, S.W. and Olejniczak, E.T. (1991) *J. Am. Chem. Soc.*, **113**, 370–372.